Microfluidic Cell Culture Chambers with Nanoporous Walls for Chemical Communication

by

Zhifei Ge

B.S. Shanghai Jiao Tong University (2010)

Submitted to the Department of Mechanical Engineering

in partial fulfillment of the requirements for the degree of

Master of Science in Mechanical Engineering

at the

MASSACHUSETTS INSTITUTE OF TECHNOLOGY

August 2013
[SEPTEMBER 2013]

Author.... .....

Department of Mechanical Engineering

August 23, 2013

Certified by.....

Cullen R. Buie

Assistant Professor

Thesis Supervisor

Accepted by.....

David E. Hardt

Graduate Officer, Department of Mechanical Engineering

Microfluidic cell culture chambers with nanoporous walls for chemical communication

by

Zhifei Ge

Submitted to the Department of Mechanical Engineering
On August 23, 2013 in partial fulfillment of the
requirements for the degree of
Master of Science in Mechanical Engineering

Abstract

Reconstruction of phylogenetic trees based on 16S rRNA gene sequencing reveals that so far only a tiny fraction of microbial diversity has been cultured in the laboratory. One major reason behind this "unculturability" is that many microbes function in symbiosis, frequently exchanging metabolites to sustain their own metabolism, while key exchanged metabolites have hardly been identified. To advance the culturability of diverse microbes we propose a method to engineer a microfluidic co-culture platform, the Microfluidic Cell Culture Chambers, which mimics natural conditions for bacterial growth. The key innovation is to physically isolate bacteria while allowing chemical communication through metabolite diffusion. In this work, the device enables both high-throughput screening and real-time observation of bacterial growth.

In our method, we use a porous material, poly(2-hydroxyethyl methacrylateco-ethylene dimethacrylate) (HEMA-EDMA), to fabricate a microwell array with 10^5 individual culture chambers. Pore size of HEMA-EDMA was confirmed by ESEM imaging to be less than 200 nm, adequate for isolating all identified bacteria. We have video-recorded fluorescence labeled *Escherichia coli* swimming in confined HEMA-EDMA wells and observed that *E. coli* is unable to travel between culture chambers. Single-strain *E. coli* is cultured with the device to test bio-compatibility of the device. Syntrophic pairs of *E. coli* were constructed to test the devices' ability to culture inter-dependent species with physical isolation.

In future work, culture of quorum sensing strains is suggested to look into inter-species chemical communication in the Microfluidic Cell Culture Chambers. The future device may be applied to recover uncultured microbial species from natural habitat.

Thesis Supervisor: Cullen R. Buie

Title: Assistant Professor

Acknowledgments

I would like first to thank my advisor, Professor Cullen Buie, for his guidance and inspirations. This thesis would not have been completed without his generous support to solve the difficult problems. Also, I would like to thank Professor Peter Girguis for his numerous advices on the biology part of the thesis.

I would also like to thank all the other lab members of the Laboratory for Energy and Microsystem Innovation. They have provided me with invaluable suggestions throughout my three years in the Institute. I must also pay particular thanks to Eric Ma who helped me go through the process of bacterial transformation and directing me to the resources of iGEM.

The last two years have been particularly hard for my family. But their understanding and support for me gives me the strength to continue working on this project.

Contents

Chapter 1. Introduction 9

1.1 Culturing the Uncultured 9

1.2 Intercellular communication 11

1.3 Purpose of the research 11

1.4 Organization of the Thesis 12

Chapter 2. Design of the Microfluidic Cell Culture Chambers 13

2.1 Introduction 13

2.2 Literature Survey 14

2.3 Design of the Microfluidic Cell Culture Chamber 15

Chapter 3. Material Characterization 17

3.1 Introduction 17

3.2 Synthesis of HEMA-EDMA 17

3.3 Microscopic Imaging of HEMA-EDMA 18

3.4 Diffusivity Measurement 20

Chapter 4. Fabrication of the Microfluidic Cell Culture Chamber 27

4.1 Introduction 27

4.2 Pre-processing of Glass Slides 29

Chapter 5. Physical Model to Predict Bacterial Population Dynamics in the Microfluidic Cell Culture Chamber 31

5.1 Introduction 31

5.2 Continuum Model (CM) 33

5.3 Individual-Based Model (IBM) 35

5.4 Simulation Results and Discussion 36

Chapter 6. Culture of Bacteria in Microfluidic Cell Culture Chambers 42

6.1 Introduction 42
6.2 Cell Seeding Protocol 42
6.3 Single Strain *E. coli* Culture 43
6.4 Construction of a Syntrophic Pair of *E. coli* 47
6.5 Co-Culture in the Microfluidic Cell Culture Chambers 49
Chapter 7. Future Work and Conclusion 50
7.1 Future Work 50
7.2 Conclusions 51
Appendix A 53
Bibliography 63

List of Figures

1.1 Distribution of cultivated species....10

2.1 Working Principle of the Co-Culture Device....13

2.2 Ideal seeding results in the co-culture device....15

3.1 ESEM image of nanoporous HEMA-EDMA. Scale bar: 1 μm....19

3.2 ESEM image of nanoporous HEMA-EDMA. Scale bar: 200 nm....19

3.3. ESEM image of microporous HEMA-EDMA. Scale bar: 5 μm....20

3.4 Design principle of the dual chamber diffusion cell....21

3.5 Breakdown of the diffusion cell....21

3.6 Image of the diffusion cell....21

3.7 UV-1800 UV/Vis spectrophotometer, Shimadzu Scientific Instruments, Inc....23

3.8 Reference curve of glycine concentration with UV adsorption at 200 nm....24

3.9 Reference curve of BSA concentration with UV adsorption at 280 nm....24

3.10 Time-lapse chemical concentration in Chamber B for glycine and BSA....25

4.1 General fabrication process of the Microfluidic Cell Culture Chambers....29

4.2 Top view of the HEMA-EDMA micro-well array under optical microscope. Scale bar, 100 μm....29

4.3 Chemistry of the glass surface treatment process....30

5.1 Field for simulation of the physical model....32

5.2 General logic in formulating the physical model....32

5.3 Nutrient concentration distribution outside of the bacterium....34

5.4 Prediction of population change from the Continuum Model when there is a single strain of bacteria in the Microfluidic Cell Culture Chambers.....37

5.5 Prediction of population change from the Individual Based Model when there is a single strain of bacteria in the Microfluidic Cell Culture Chambers.....38

5.6 Population change prediction from the CM when two syntrophic strains of bacteria are seeded into the Microfluidic Cell Culture Chambers and are neighbors to each other.....39

5.7 Population change prediction from the IBM when two syntrophic strains of bacteria are seeded into the Microfluidic Cell Culture Chambers and are neighbors to each other.....40

5.8 physical occupancy by bacteria for asymmetric symbiosis simulation.....41

5.9 population change prediction for bacteria residing in the three types of wells when two syntrophic strains of bacteria are seeded into the Microfluidic Cell Culture Chambers and occupy unequal amount of space.....41

6.1 Protocol for seeding bacteria into the Microfluidic Cell Culture Chambers.....43

6.2 Two snapshots from a video of one bacterium inside a chamber immediately after the bacteria are seeded into the device.....45

6.3 Images of the single-strain *E. coli* culture process. a) Immediately after the bacteria are seeded; b) After about six hours' culture; c) After about 12 hours' culture.....47

6.4 Protocol for co-culture of *E.coli* Δ*arg* and Δ*cys*.....49

7.1 Working principle of quorum sensing pairs.....50

Chapter 1. Introduction

1.1 Culturing the Uncultured

Since the use of 16S rRNA sequencing in sketching the phylogenetic diversity of bacteria[1, 2, 3], knowledge of the estimated bacterial diversity has increased significantly. In the late 1970s and early 1980s, 11 phyla of bacteria were recognized by Woese and co-workers[4, 5, 6]. In 2003, the number of identified bacterial phyla has been increased to 52[7]. An estimate done by Curtis and co-workers[8] speculated that the number of bacterial species living in the sea may be less than 2×10^6, while a ton of soil can contain as many as 4×10^6 bacterial species. This large pool of bacterial diversity[9, 10] provides enormous natural products to search for drugs, such as antibiotics[11].

Unfortunately, most of the bacterial species are yet to be cultured in lab. As of 2004, there were 4856 cultivated species[12]. Contrasted with the vast number of bacterial species estimated by Curtis and co-workers, the cultured species represent only a tiny proportion. Moreover, as shown in Fig. 1.1, most of the cultured species lie in 5 phyla, *actinobacteria*, *bacteroidetes*, *firmicutes*, *proteobacteria* and *spirochaetes*. These 5 phyla account for about 97% of all cultivated species, and 25 recognized bacterial phyla contain no cultured representatives at all.

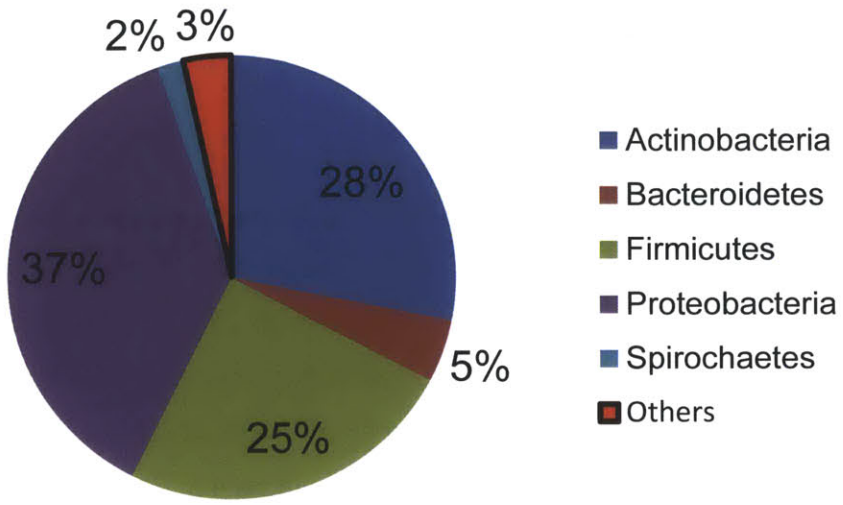

Fig. 1.1 Distribution of cultivated species[12].

In fact, the inability to culture a majority of bacteria was observed by H. Winterberg in 1898[13]. In the experiment done by Winterberg, an environmental sample was diluted and plated on a Petri dish with LB medium. The number of colonies formed on the Petri dish did not match the number of microbial cells in his sample. This microbiological phenomenon was named as the Great Plate Count Anomaly by Staley and Konopka in 1985[14].

One clue to the puzzle of the Great Plate Count Anomaly is that the Petri dish with LB medium fails to replicate some essential aspects of the bacterial living environment[12]. For example, bacteria in nature do not live alone. Instead, they live in a community with a lot of other species. Those bacteria that live in a community may obtain some critical nutrients or chemicals from other species. When cultured in isolation in lab, bacteria do not get those necessary nutrients from LB broth or other medium used by researchers in lab. As an example, in the research done by A. D'Onofrio and co-workers[15], it is discovered that some cultured bacteria can help previously uncultivated bacteria grow by producing and feeding the latter with siderophores. Siderophores are not contained naturally in LB broth. Therefore, if we try to use LB broth to recover those bacteria in isolation, we are likely to fail.

1.2 Intercellular communication

In a naturally formed microbial community, microbial interactions are more abundant than just cross-feeding[16]. Pair wise interactions include parasitism, amenalism, competition, mutualism, and commensalism[17], depending on how either of the pair benefit from the existence of the other. With metagenomics and 16S pyrosequencing, we are able to obtain abundant data about the evolution of the community. With appropriate modeling[18, 19], we can predict microbial relationships and then the ecological structure within the studied microbial community[16]. However, the dilemma is that with the same data, different model can lead to significantly different predictions about relationships between two species in a community[20]. One main reason is that these models cannot tell true ecological interactions from nonrandom activities. To distinguish these possibilities, more experimental data, such as metabolic data, should be collected and analyzed[21, 22].

With input from the ecological modeling of naturally formed microbial communities, an artificially constructed community in a co-culture setup provides ideal conditions to test and validate these ecological models, especially if the environment of the constructed community is well controlled and measured[16]. Becks and co-workers[23, 24] use co-culture experiments to demonstrate chaotic behavior in a three-species system. Down the line, in order to study more complicated microbial systems, a high-throughput co-culture system that is integrated with proper measurement techniques is required.

1.3 Purpose of the research

In both cultivation of uncultured species and study of inter-species communication, there is a call for a multispecies experimental system. The requirement of the system is well summarized by P. Straight and R. Kolter[25]:

"Developing multispecies experimental systems that incorporate knowledge of bacterial physiology and metabolism with insights from biodiversity and metagenomics shows great promise for understanding interspecies chemical communication in the microbial world."

In this work, we are developing a device called Microfluidic Cell Culture Chambers. The Microfluidic Cell Culture Chambers are capable of co-culturing multiple species of bacteria in

physical isolation while retaining inter-species chemical communication. The key innovation is our Microfluidic Cell Culture Chambers enable simultaneous high-throughput screening and real-time observation.

We envision that the Microfluidic Cell Culture Chambers can be applied to isolate uncultivated species, and used in experimental validation of microbial network models.

1.4 Organization of the Thesis

The Thesis is organized into seven chapters. Followed the general introduction in Chapter 1, Chapter 2 will discuss the state of art in building co-culture systems and the design principle of the Microfluidic Cell Culture Chambers.

Chapter 3 will discuss the key materials, poly(2-hydroxyethyl methacrylateco-ethylene dimethacrylate) (HEMA-EDMA), used to build the device. HEMA-EDMA is a kind of hydrogel. Extensive characterization of HEMA-EDMA is presented in Chapter 3 to justify its application in building the co-culture system.

Based on Chapter 2 and 3, Chapter 4 presents the replica molding fabrication process to build the Microfluidic Cell Culture Chamber.

In Chapter 5, physical models are built to predict bacterial population dynamics with the device. Three different scenarios are assumed to predict how bacterial populations evolve in the Microfluidic Cell Culture Chambers.

Followed by numerical models, Chapter 6 presents the biological experiments. In this chapter, both single-strain and multi-strain experiments are presented.

Chapter 7 concludes the Thesis and suggests future work.

Chapter 2. Design of the Microfluidic Cell Culture Chambers

2.1 Introduction

In typical co-culture systems, bacteria of different species are isolated physically by porous walls[26]. The pore size is small enough so that bacteria cannot cross the wall, while the pore is large enough to let metabolites secreted by bacteria pass through. In this way, bacteria of different species are physically segregated while inter-species chemical communication is retained.

As shown schematically in Fig. 2.1, Organism 1 is seeded in the Chamber 1 and Organism 2 in Chamber 2. The wall separating Chamber 1 and Chamber 2 is made up of nanoporous materials. Both Organism 1 and Organism 2 are unable to cross the nanoporous membrane. However, metabolites secreted by Organisms 1 and 2 can cross the nanoporous membrane. During culture, Organisms 1 and 2 can secrete metabolites. These metabolites can diffuse across the nanoporous membranes and be absorbed by the other species. By observing each chamber constantly, we can measure bacterial population change in bacterial growth. This growth data can be used to validate inter-species chemical communication model. After culture, we can harvest pure samples of each species by carefully isolating bacteria from each chamber separately.

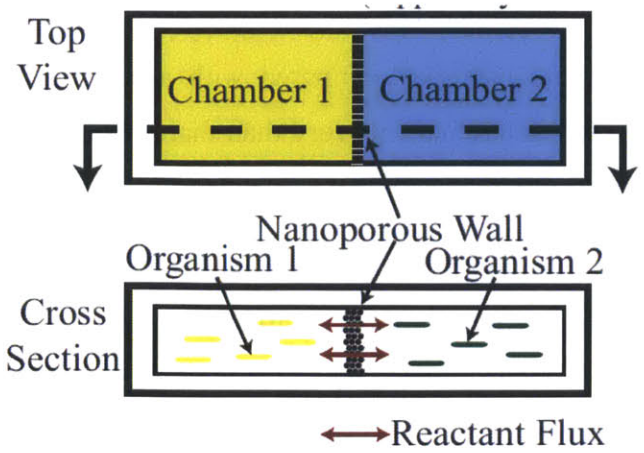

Fig. 2.1 Working Principle of the Co-Culture Device

2.2 Literature Survey

The first co-culture system to cultivate uncultivated microorganisms was designed by S.S. Epstein and co-workers[27]. In their system, the diffusion growth chamber is formed by a washer sandwiched between two polycarbonate membranes. The specified pore size of the polycarbonate membranes by the manufacturer is 0.03 μm. Diffusion chambers were incubated in an aquarium to simulate bacteria's natural living environment. Marine microorganism culture that was previously uncultured was isolated. An upgraded device was designed by the same group called isolation chip (ichip)[28]. The ichip was fabricated by sandwiching flat plastic plates with porous membranes. The flat plastic plates contain arrays of through-holes with a diameter of 1 mm. The through-holes are chambers for isolated culture of bacteria. Again, Epstein and co-workers observed that microbial recovery in the ichip significantly exceeds that in standard cultivation.

A high-throughput co-culture method was developed by Zengler and co-workers based on gel microcapsulation and flow cytometry[29]. In Zengler's method, single cells were encapsulated into agarose gel microcapsules, while agarose was cured at the same time. Samples from both seawater and soil led to cultures that were previously uncultivable.

An upgraded version of Zengler's method was designed by E. Ben-Dov and co-workers[30]. In Ben-Dov's method, cell-containing agar spheres are coated with polysulfone. The polysulfone serves as better walls to isolate bacteria, compared with agar. E. Ben-Dov and co-workers observed 10 to 100 fold greater microbial recovery than that possible with conventional plating techniques.

The concept to physically isolate cells while retaining intercellular chemical communication has been furthered to facilitate *in situ* observations. In 2007, C. Ingham and co-workers designed a micro-Petri dish[31], a million-well growth chip for culturing segregated microbial samples. C. Ingham et al used fluorescence microscopy to screen cultures. In one high-throughput screening of an environmental sample from the Rhine River, six new intractable species were cultured.

However, C. Ingham's million-well growth chip floats on sheep's blood agar in a standard Petri dish and thus is not ameable for real-time observations.

A co-culture system with capability for real-time observation was proposed by Y. Cheng and co-workers[32]. In this system, alginate gels are cured locally by local pH change triggered electrically with addressable electrodes. Locally cured alginate gels entrap cells during gelation. By changing the cell solution and triggering alginate gelation at different time, Y. Cheng and co-workers are able to encapsulate different cells at different locations and thus segregating cells of different species. A pair of strains--with one strain sending quorum sensing molecules and the other reporting receipt of the quorum sensing molecules by expressing red fluorescence proteins--was cultured with the microfluidic device to demonstrate the capability of the device to interrogate cell signaling.

2.3 Design of the Microfluidic Cell Culture Chamber

The methods and devices reviewed in the last sections are either high-throughput or real-time. None of them have combined the capability of high-throughput screening and real-time observation. In our design, both features are captured. The advantage of being both high-throughput and real-time is the abundant real-time data generated during culturing process. This data can be used to generate more insights into the microbial community of interest.

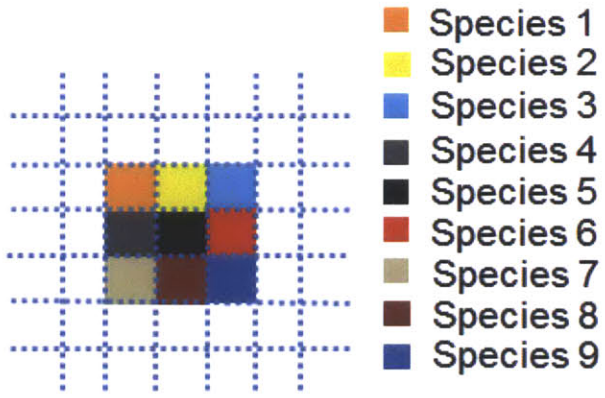

Fig. 2.2 Ideal seeding results in the co-culture device

In our design, we use nanoporous hydrogels to create multi-well patterns on the glass. Every well is a chamber for isolated culture of bacteria. As shown conceptually in fig. 2.2, when seeded ideally, each species of bacteria can occupy a well and grow within the well. Bacteria cannot cross the nanoporous hydrogel walls, but metabolites released by the bacteria can cross the nanoporous walls. Therefore, bacteria are physically isolated while inter-species chemical communication is retained.

The nanoporous walls are fabricated with replica molding of soft lithography. This fabrication process is easily scalable (detailed fabrication process is described in Chapter 4.) With soft lithography[33, 34], resolution of 10 μm is easily within reach. This means that with each chamber dimension of 100 μm x 100 μm x 100 μm and wall width 50 μm, we can create 10,000 wells in only a few square centimeters. With this highly scalable process, we can fabricate a high-throughput microfluidic device for co-culture.

The advantage of using glass as the substrate is that the device will be compatible with optical microscopy. For example, if the bacteria are able to express fluorescent proteins, we can measure fluorescence intensity change in real time. In this way, we can use fluorescent data to measure the bacterial growth. In another application, the fluorescent intensity may be used to analyze inter-species chemical exchange. For example, in a quorum sensing system used by Cheng and co-workers[32], expression of green fluorescent proteins is connected with sensing of autoinducer-2 molecules. Detection of green fluorescence means successful communication of the autoinducer-2 molecules.

Chapter 3. Material Characterization

3.1 Introduction

Hydrogels, or hydrophilic polymers, were first discovered by Wichterle and Lim in 1960[35]. Since then, there have been significant advancements in hydrogel research. Several types of hydrogels have been widely explored for their synthesis and applications, such as poly(hydroxyethyl methacrylate) (PHEMA), poly(ethylene glycol) (PEG), and poly(N-isopropylacrylamide) (PNIPAAm). In particular, hydrogels have been widely studied and used in biomedical applications[36, 37] such as contact lenses[38] and for drug delivery[39].

In this research, we use the hydrogel of poly(2-hydroxyethyl methacrylateco-ethylene dimethacrylate) (HEMA-EDMA). We characterized HEMA-EDMA extensively before using it to build the microfluidic device.

3.2 Synthesis of HEMA-EDMA

Hydrogels are synthesized by cross-linking monomers. In the precursor solution for synthesizing hydrogels, there are monomers, cross-linkers and solvent. The amount and composition of solvent in the precursor solution influences the effective pore size of the synthesized hydrogel. The precursor solution is mixed according to that described by F. Geyer and co-workers[40].

In the precursor solution to synthesize nanoporous HEMA-EDMA, we have: 2-hydroxyethyl methacrylate (HEMA, Sigma-Aldrich) (24 %wt.), ethylene dimethacrylate (EDMA, Sigma-Aldrich) (16 %wt.), 1-decanol (Sigma-Aldrich) (12 %wt.), cyclohexanol (Sigma-Aldrich) (48 %wt.) and 2,2-dimethoxy-2-phenylacetophenone (Sigma-Aldrich) (DMPAP) (1 %wt.)

In the precursor solution to synthesize microporous HEMA-EDMA, we have: 2-hydroxyethyl methacrylate (HEMA) (24 %wt.), ethylene dimethacrylate (EDMA) (16 %wt.), 1-decanol (40 %wt.), cyclohexanol (20 %wt.) and 2,2-dimethoxy-2-phenylacetophenone (DMPAP) (1 %wt.) Compared with the precursor solution for nanoporous HEMA-EDMA, only the concentration of 1-decanol and cyclohexanol have been changed.

HEMA-EDMA is photo-cross-linked. In the precursor solution, HEMA and EDMA are the monomers. DMPAP is the photo-initiator. 1-decanol and cyclohexanol are solvent.

3.3 Microscopic Imaging of HEMA-EDMA

After HEMA-EDMA is fabricated, samples of HEMA-EDMA are prepared for Environmental Scanning Electron Microscopy (ESEM) (FEI/Philips XL30 FEG ESEM). With normal SEM, we need to deposit gold on top of the sample to render the materials conductive. With ESEM, this step can be eliminated. Before putting samples into the vacuum chamber of the ESEM, samples are kept in a normal vacuum chamber for several hours. The reason for this step is there are always 1-decanol and cyclohexanol left inside the cross-linked hydrogel. These leftover molecules can evaporate under vacuum. Without vacuum processing, the vacuum level in the vacuum chamber of the ESEMcannot be decreased to the level necessary for imaging.

Fig. 3.1 (scale bar 1 μm) and fig. 3.2 (scale bar 200 nm) shows the structure of nanoporous HEMA-EDMA. Fig. 3.3 (scale bar 5 μm) shows the microscopic imaging of the microporous HEMA-EDMA.

Fig. 3.1 and fig. 3.2 indicate that the pore size of the nanoporous HEMA-EDMA is always smaller than 200 nm, which is smaller than the size of the smallest bacteria that have been identified so far. Therefore, the nanoporous HEMA-EDMA is very promising for physically isolating bacteria.

On the other hand, with the scale bar at 5 μm, it is evident that many pores of the microporous HEMA-EDMA are greater than 200 nm. However, since the pores inside the material are very tortuous, ESEM images are insufficient evidence that the microporous HEMA-EDMA cannot physically isolate bacteria. Biological experiments are presented in later chapters to confirm that microporous HEMA-EDMA indeed cannot physically isolate bacteria.

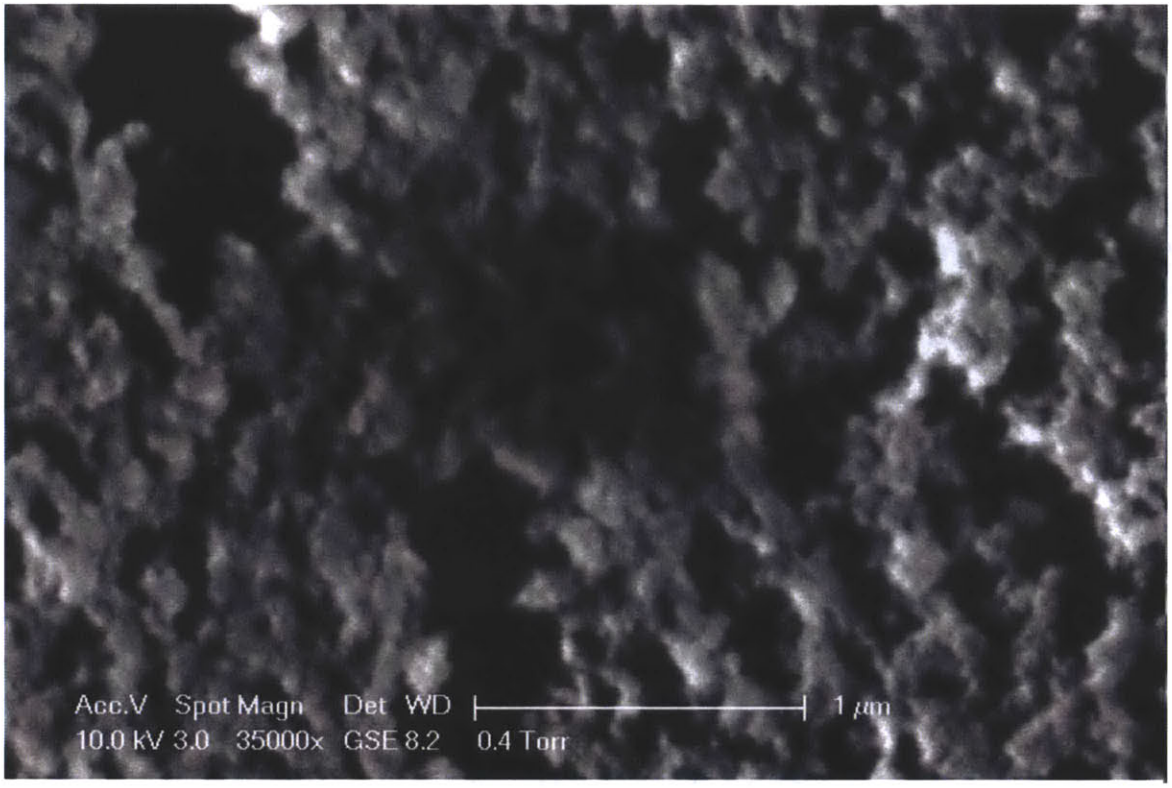

Fig. 3.1 ESEM image of nanoporous HEMA-EDMA. Scale bar: 1 μm

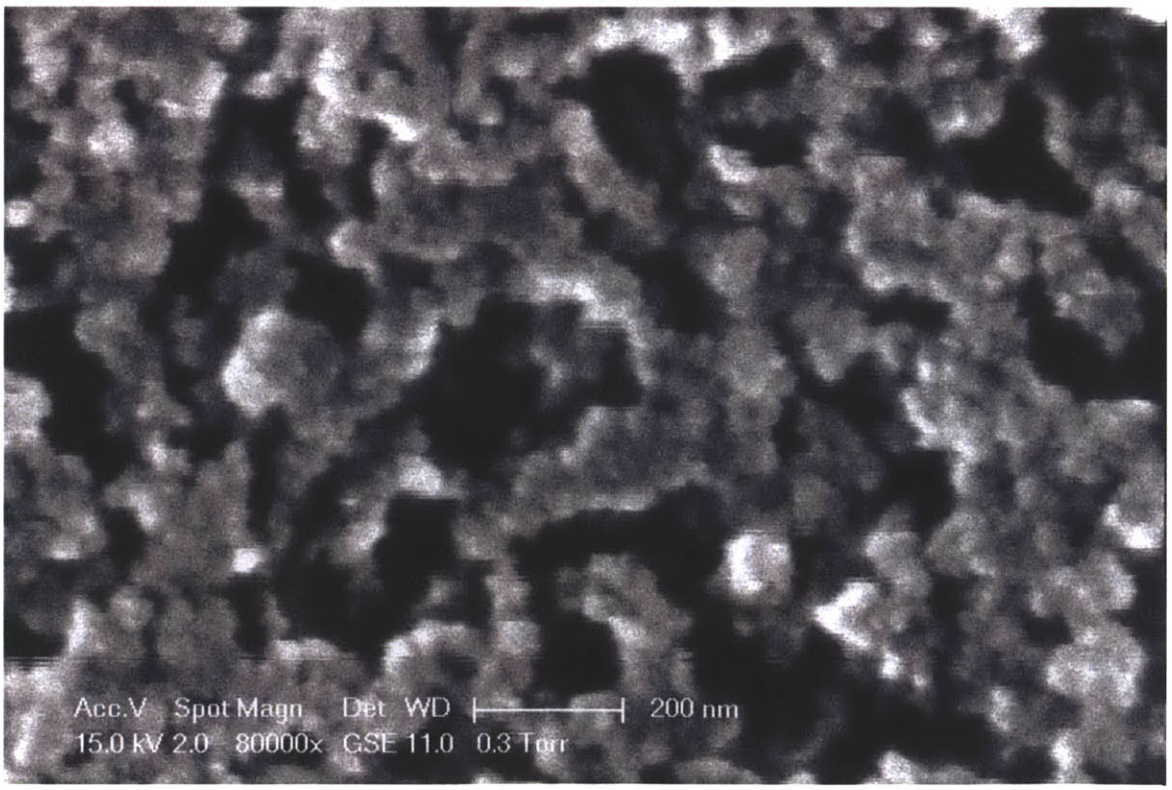

Fig. 3.2. ESEM image of nanoporous HEMA-EDMA. Scale bar: 200 nm

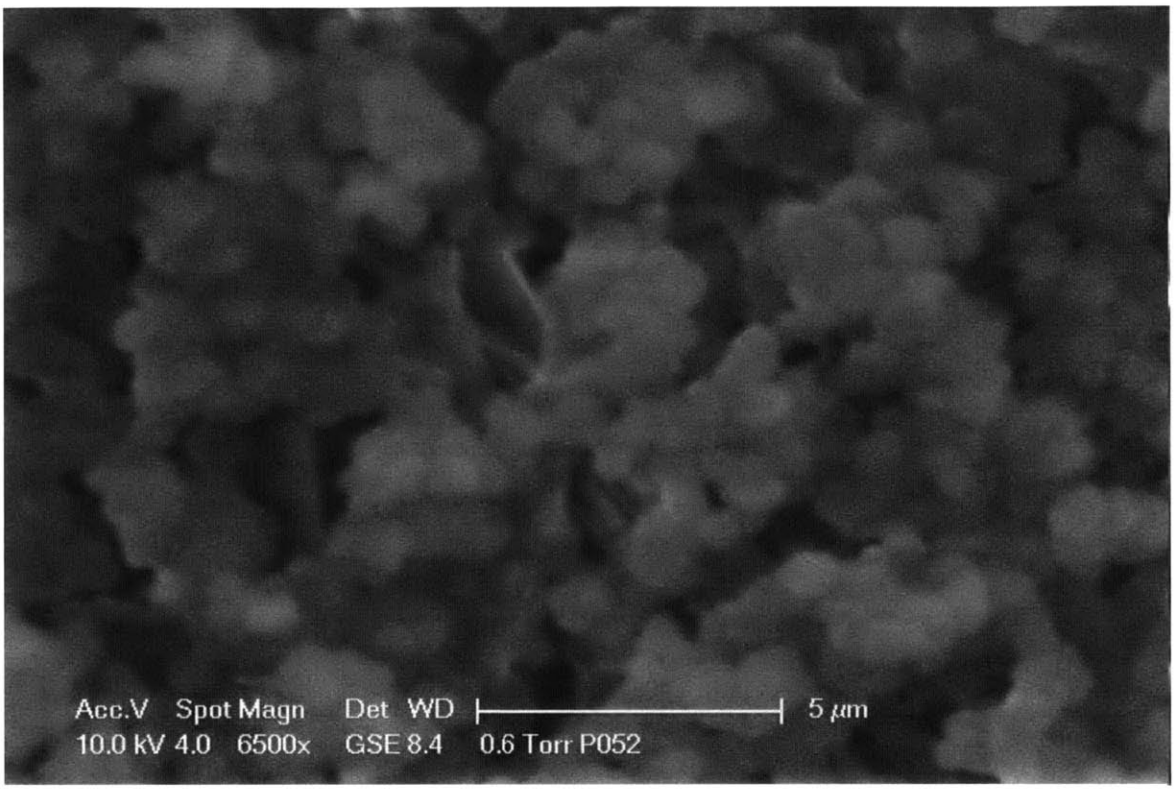

Fig. 3.3. ESEM image of microporous HEMA-EDMA. Scale bar: 5 μm

3.4 Diffusivity Measurement

3.4.1 Design of the Diffusivity Measurement Experiment

As pointed out in Chapter 2, metabolites or chemicals released by bacteria will diffuse across the membrane. The diffusivity of the chemicals across the membrane is a key parameter in determining the flux of chemicals received by the other species. In this section, a customized dual chamber diffusion cell is proposed to measure diffusivity of two representative molecules, glycine and bovine serum albumin (BSA), across the nanoporous and microporous membranes presented in the last section.

The design principle of the dual chamber diffusion cell is shown in Fig. 3.4. Dilute solution of certain molecule is seeded in Chamber A and deionized water in Chamber B. If the membrane is permeable to the molecule, the molecule will diffuse across the membrane and the concentration of the molecule in Chamber B will increase.

The actual design of the diffusion cell is shown in Fig. 3.5 and Fig. 3.6. The cell is built with acrylic plates. Fig. 3.5 is the breakdown of the diffusion cell. The membrane is inserted in-between before the two components are brought together.

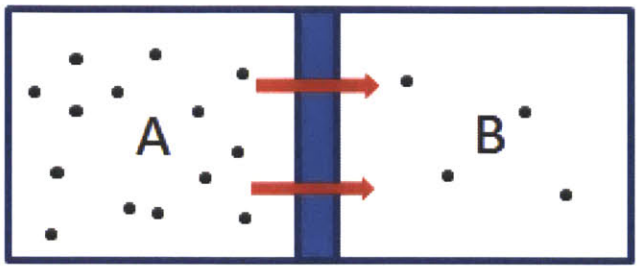

Fig. 3.4 Design principle of the dual chamber diffusion cell

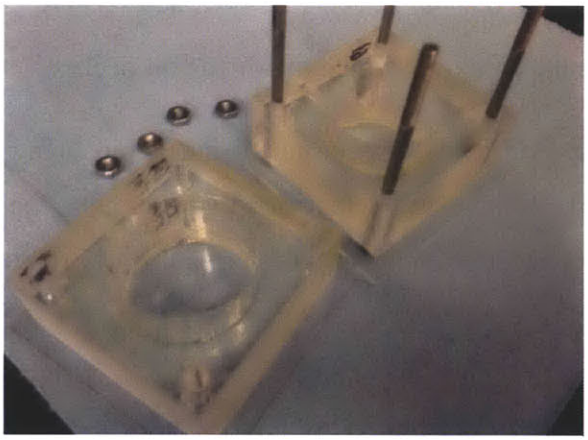

Fig. 3.5 Breakdown of the diffusion cell

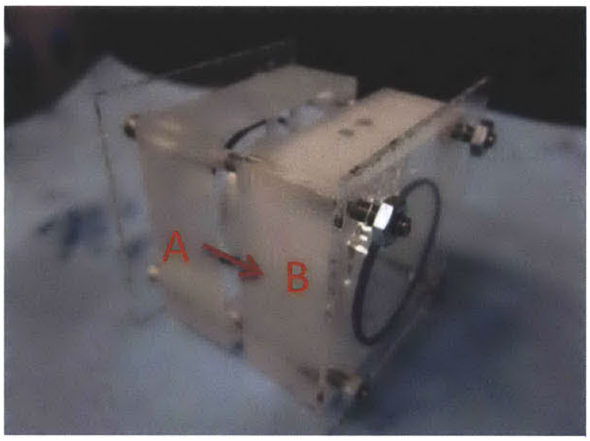

Fig. 3.6 Image of the diffusion cell

According to the transport theory of dilute solutions, concentration of molecules in chamber B follows a time-dependent diffusion model[41]:

$$-\ln\left(1-\frac{C_B(t)}{C_\infty}\right)=\frac{D}{h}\left(\frac{t}{\tau}\right) \tag{3.1}$$

Where $C_B(t)$ is the chemical concentration in Chamber B;

C_∞ is chemical concentration in long-term steady state in chamber B, in the case of each chamber size and diffusible molecule across the membrane, C_∞ is just half the initially seeded concentration of the chemical in Chamber A;

D is the effective diffusivity;

h is the membrane thickness;

t is time;

V and τ are geometric parameters according to the following correlations[41]:

$$V = V_1 + Ah + V_2 \tag{3.2}$$

$$\tau = \frac{(V_1 + Ah/2)(V_2 + Ah/2)}{AV} \tag{3.3}$$

V_1 and V_2 are the volume of the two chambers. A is the area over which the diffusion occurs.

The solution in chamber B is constantly sampled, and its UV spectrum is measured using a UV/Vis spectrophotometer (Fig. 3.7, UV-1800, Shimadzu Scientific Instruments, Inc.). According to the Beer-Lambert law[42], chemical concentration of the solution is linearly related to UV adsorption.

$$A(t) = \epsilon \cdot l \cdot C_B(t) \tag{3.4}$$

Where, $A(t)$ is UV absorption measured by the UV/Vis spectrophotometer;

ϵ is molar absorptivity;

l is the pathlength through the sample.

At dilute concentration of the solution, ϵ and l are both fixed constants. Thus, absorption A will be linear with respect to chemical concentration $C_B(t)$.

Thus, measuring the time-lapse UV absorption of the solution, we can derive the time-lapse chemical concentration in Chamber B. After obtaining the time-lapse concentration, the

concentration curve can be fit with the time-dependent diffusion model to derive the diffusivity across the HEMA-EDMA membrane.

Fig. 3.7 UV-1800 UV/Vis spectrophotometer, Shimadzu Scientific Instruments, Inc.

3.4.2 Reference Curve for the Chemical Concentration-UV absorption Correlation

Two representative molecules--glycine and BSA--have been measured for their diffusivity across the nanoporous and microporous membranes. Glycine, with its molecular formula as NH_2CH_2COOH, has a molecular weight of 75 Da. In contrast, BSA, a serum albumin protein derived from cows, has a molecular weight of ~66 kDa.

The reference curve for the chemical concentration-UV absorption correlation is obtained by measuring the UV absorption of the solution at known chemical concentration. Fig. 3.8 gives the correlation of glycine concentration with UV adsorption at 200 nm. Every point in the figure is an average of two measurements. Fig. 3.9 gives the correlation of BSA concentration with UV adsorption at 280 nm. Different wavelengths of UV light are picked to maximize light adsorption. From these curves, we can derive the mathematical dependence of UV absorption on chemical concentration.

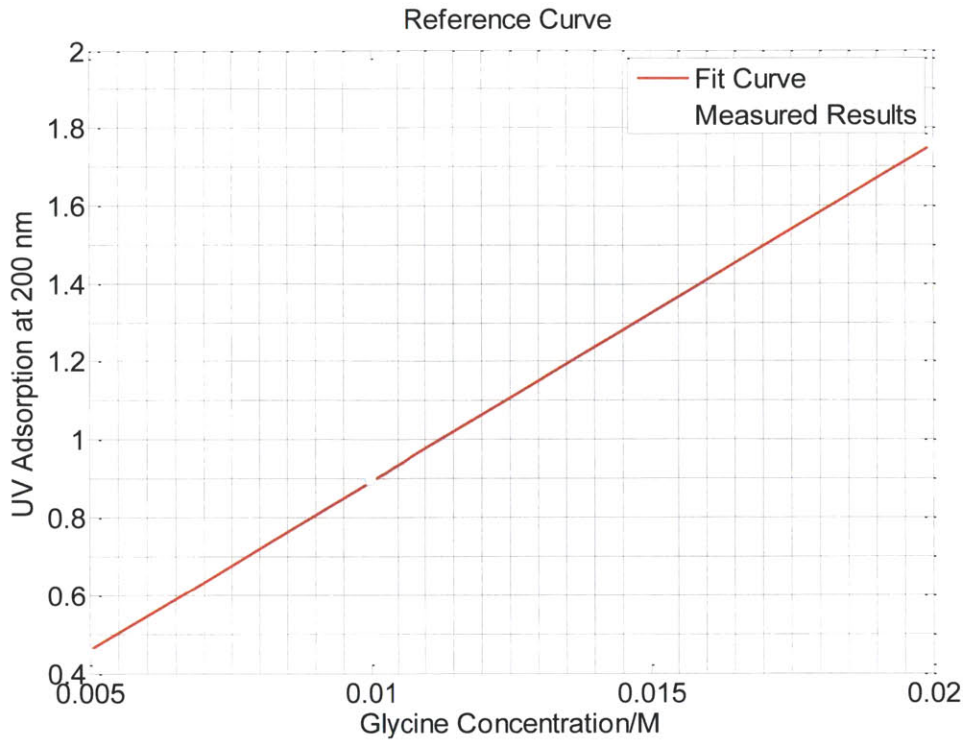

Fig. 3.8 Reference curve of glycine concentration with UV adsorption at 200 nm

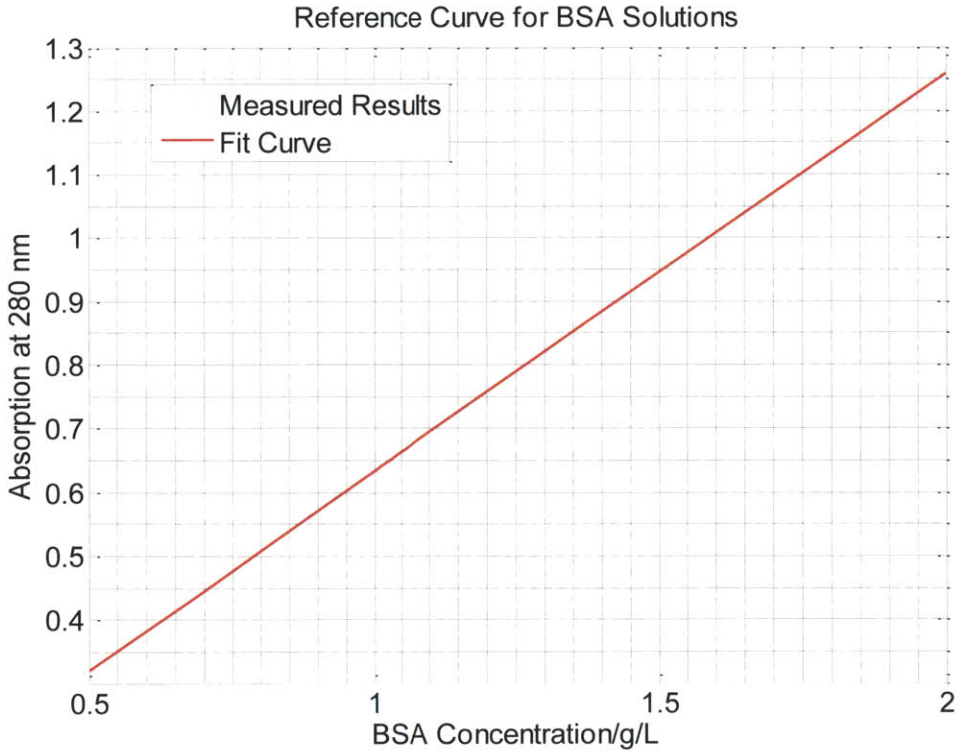

Fig. 3.9 Reference curve of BSA concentration with UV adsorption at 280 nm

3.4.3 Time-Lapse Diffusion

Mechanically, HEMA-EDMA is not strong enough to make a two-inch long membrane. A supporting structure, in this case a glass fiber filter membrane (size 47mm, Pall Corporation), is used to support HEMA-EDMA. That is, HEMA-EDMA is crossed-linked with the glass fiber membrane as the substrate.

The size of Chamber A and B are 1.5 inch (38.1 mm) in diameter with the height 1 inch (25.4 mm). The thickness of the nanoporous and microporous membrane is measured with a caliper, which ranges from 0.40 mm to 0.70 mm. Every 30 min, 150 μL of solution from chamber B is sampled and its UV adsorption spectrum is measured. The concentration at that point is calculated with the help of the reference curve. Then, the time-lapse chemical concentration in Chamber B is plotted and the fit curve as done with Equation (3.1), and shown in Fig. 3.10 for the nanoporous membrane.

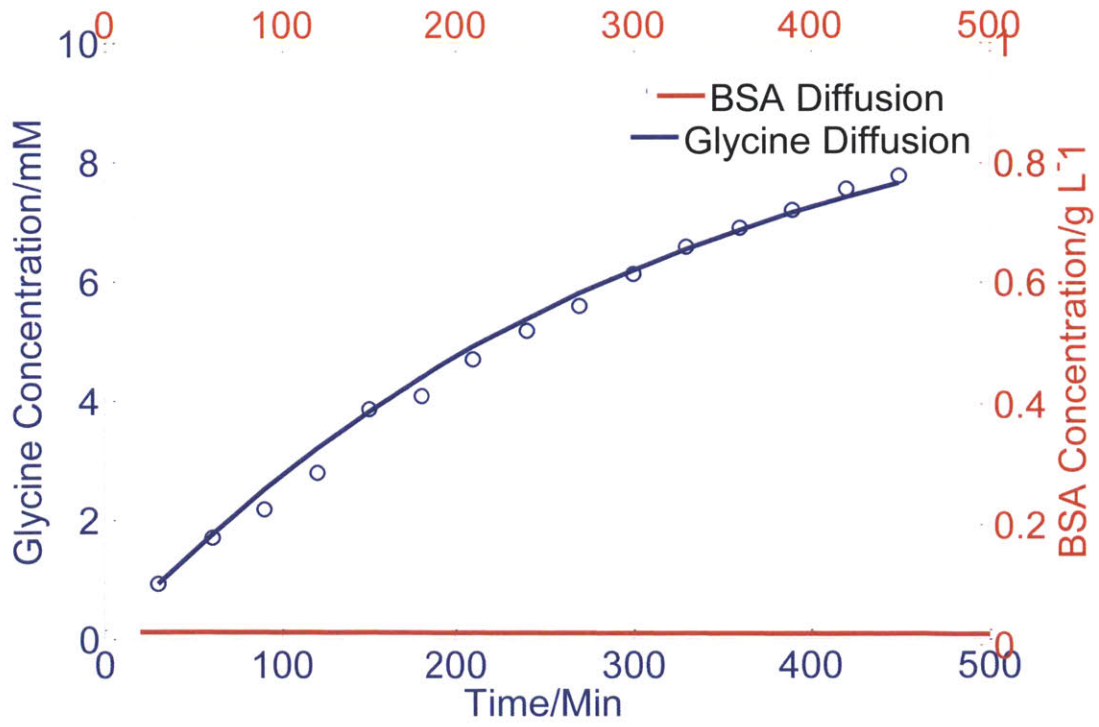

Fig. 3.10 Time-lapse chemical concentration in Chamber B for glycine and BSA

For the nanoporous membrane, the fitting result gives an effective diffusivity of glycine across the HEMA-EDMA membrane as 4.7×10^{-10} m^2/s, and ~ 0 m^2/s for BSA.

For the microporous membrane, the fitting result gives an effective diffusivity of glycine across the HEMA-EDMA membrane as 4.1×10^{-10} m^2/s, and ~ 8.0×10^{-11} m^2/s for BSA.

Since the glycine is permeable to both the nanoporous and microporous membranes and diffusivity of glycine is similar for both membranes, it indicates that overall porosity of the nanoporous and microporous membranes are similar. BSA is almost non-diffusive through the nanoporous membrane while diffusible through the microporous membrane. This indicates that the pore size of the nanoporous and microporous membranes are different, which is consistent with the ESEM imaging.

3.4.4 Culture of Fluorescent Bacteria

The above characterizations, including ESEM and diffusion test, show the distinction in diffusion properties between the nanoporous and microporous membranes, but there is insufficient evidence that bacteria cannot cross either membrane.

The same dual chamber diffusion cell is used here to culture two kinds of bacteria. These two kinds of bacteria express different fluorescent proteins, one expressing green fluorescent proteins (GFP) and the other red fluorescent proteins (RFP). Bacteria expressing GFP are seeded into Chamber A and bacteria expressing RFP Chamber B. After overnight culture, cell solution in each chamber can be sampled and observed under fluorescence microscopy.

It is observed that with the nanoporous membrane, bacteria remain segregated, while with the microporous membrane, bacteria are mixed. Therefore, to culture bacteria with physical isolation, the microporous membrane cannot be used for building the microfluidic device.

Chapter 4. Fabrication of the Microfluidic Cell Culture Chamber

4.1 Introduction

We use a polydimethylsiloxine (PDMS) mold to create multiple arrays of HEMA-EDMA micro-sized wells on glass slides. Each well is a chamber for culturing bacteria. The walls of the chamber are made of nanoporous HEMA-EDMA, so bacteria cannot swim but solute can diffuse across the walls. The micro-well arrays are patterned on glass slides to facilitate observation, especially when using the optical microscope.

The general fabrication process is shown in Fig. 4.1.

First, from Step 1 to Step 2, SU-8 (SU-8 2050, Microchem) mold is made on silicon wafer by photo-lithography. Negative photoresist is a kind of viscous liquid and is spin-coated on top of the silicon wafer for 3 min at a rotating speed of 1.7 krpm. This will lead to a uniform SU-8 film on silicon wafer with a thickness of about 100 μm. The silicon wafer with SU-8 is soft-baked at 65°C for 5 min and then at 95 °C for 15 min. Then, the wafer with SU-8 is exposed to UV light through a photomask for 23 seconds twice with 30 seconds break in-between. After exposure to UV light, the wafer is post-baked at 65°C for 4 min and then at 95 °C for 9 min. Next, the wafer with SU-8 is developed with propylene glycol monomethyl ether acetate (PM acetate). During development, the wafer is fixed on the spin-coater and rotating at 300 rpm, while PM acetate is sprayed on top of the wafer. Development lasts about 10 min. Then, isopropyl alcohol is sprayed to clean the wafer and a nitrogen gun is used to dry the surface.

Second, from Step 3 to Step 4, PDMS reverse mold is made out of the SU-8 mold. PDMS elastomer (Dow Corning Sylgard 184) is a two-part room temperature vulcanization (RTV) elastomer. It is rubberized by monomer cross-linking starting at room temperature. The two parts of PDMS elastomer are mixed at a ratio of 10:1 as specified by the manufacturer. The hand mixed PDMS elastomer is machine mixed for 1 min and degassed for 2 min in a mixer and degassing machine (THINKY ARE-250, UK). A 2-3 mm deep layer of PDMS is cast onto the silicon wafer with cured SU-8 in a Petri dish. The Petri dish is put inside a vacuum chamber for

30 min to eliminate bubbles, and then transferred to the oven set at 80 °C. The PDMS is cured in the oven for three hours before being peeled off the silicon wafer.

Third, the PDMS mold is used to create HEMA-EDMA hydrogel micro-well arrays on the glass slide. The glass slide is first functionalized with methacrylate groups. The detailed treatment process is described in Section 4.2. The precursor solution for nanoporous HEMA-EDMA is mixed with the ratio specified in Section 3.2. The precursor solution fills the space between the PDMS mold and the glass slide. The whole structure is exposed to UV light for 14 min under a UV lamp (Spectroline EA-160, Fisher Scientific, USA). Then, the PDMS mold is peeled off from the glass slide. The glass slide with cured HEMA-EDMA on top is washed with methanol and stored in methanol prior to use. Fig. 4.2 shows the HEMA-EDMA micro-well array under optical microscope (top view, scale bar in the figure is 100 μm).

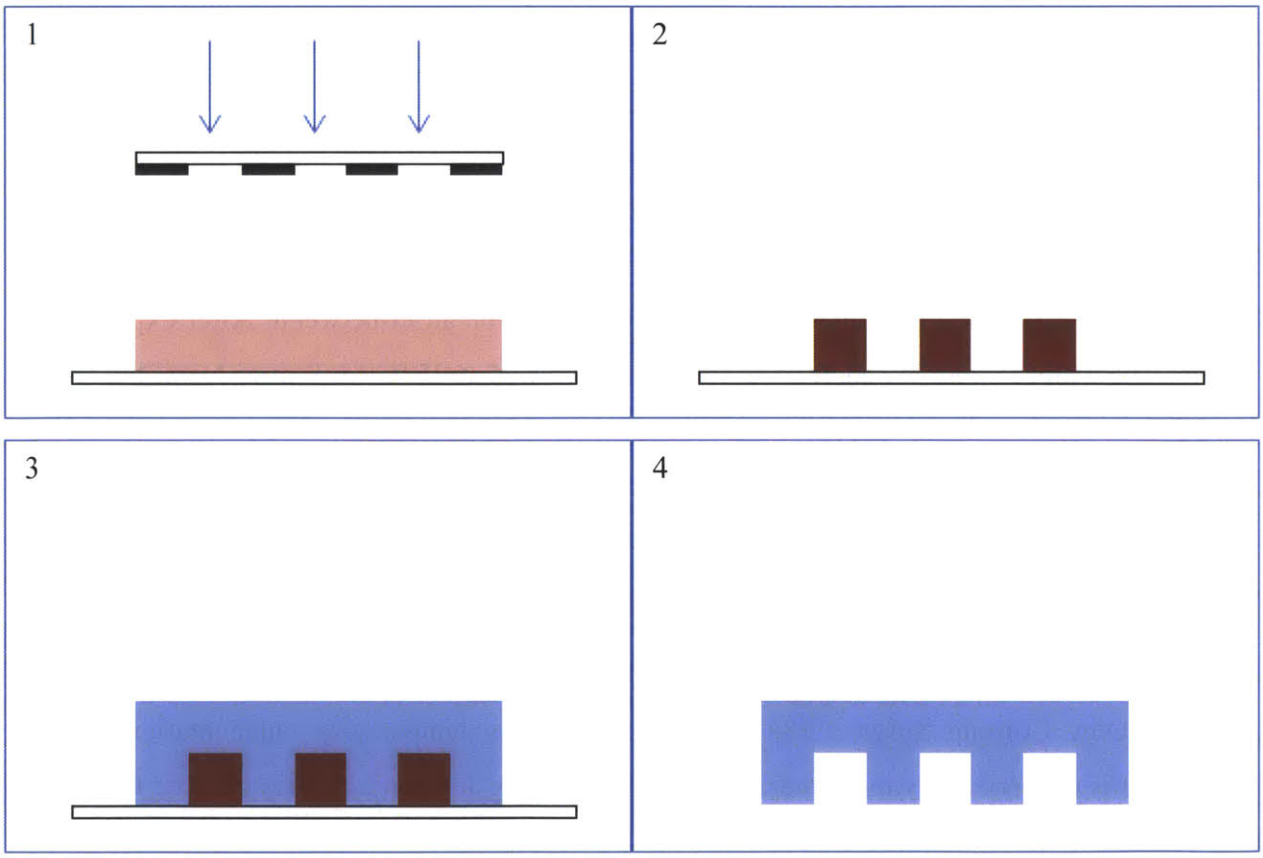

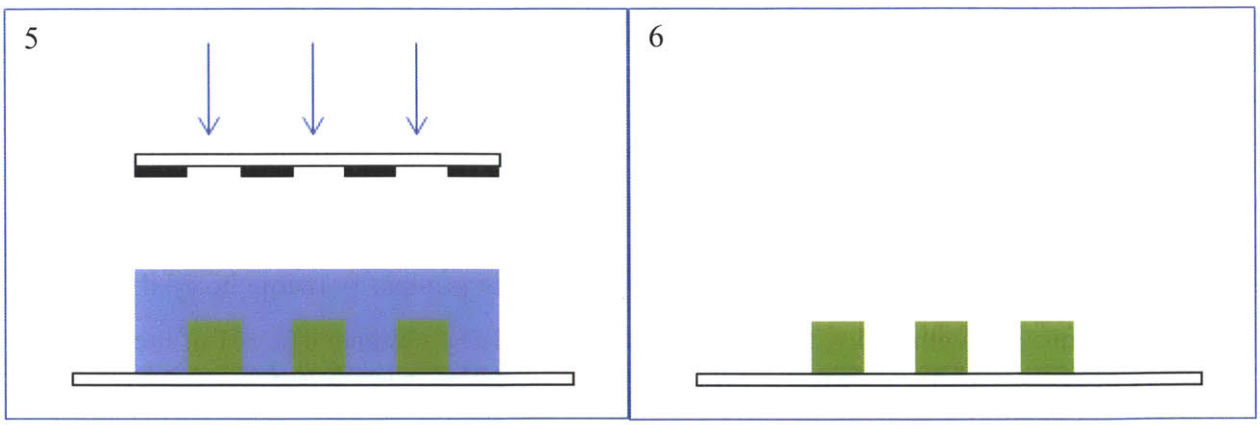

Fig. 4.1 General fabrication process of the Microfluidic Cell Culture Chambers

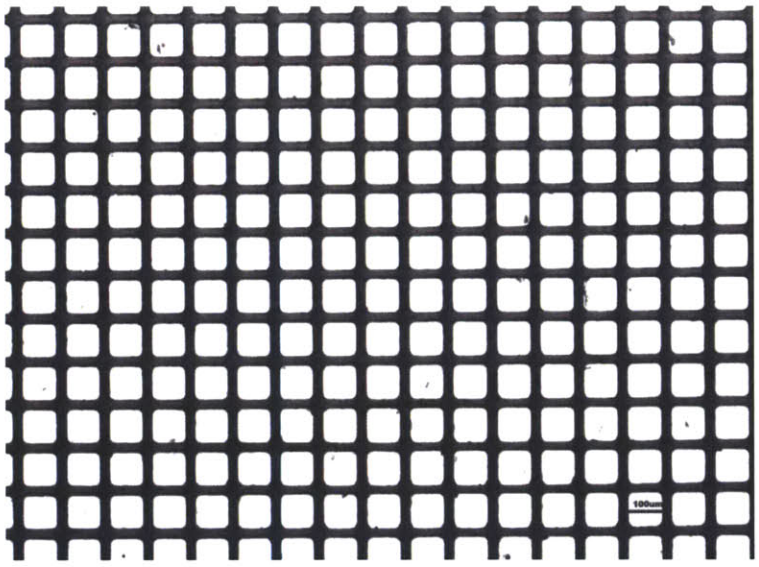

Fig. 4.2 Top view of the HEMA-EDMA micro-well array under optical microscope. Scale bar, 100 μm.

4.2 Pre-processing of Glass Slides

HEMA-EDMA does not naturally bond to the glass surface covalently. Thus, during shrinking and swelling, HEMA-EDMA can detach easily from the glass surface. In order to attach HEMA-EDMA covalently to the glass surface, the surface is first treated with 3- (trimethoxysilyl)propyl methacrylate (Sigma Aldrich) to be functionalized with methacrylate groups[43, 44], as shown in Fig. 4.3. Methacrylate groups can be covalently bonded with HEMA-EDMA if it is photo-cross-linked on top of the treated glass slide. The detailed steps are described below.

First, the glass surface is cleaned to render only hydroxyl groups. The glass slide is immersed with 1 M NaOH for 1 hour and then washed with deionized water. After the glass surface is dried with a nitrogen gun, the glass slide is immersed in 1 M HCl for 30 minutes. Then, the glass surface is washed with deionized water and dried with a nitrogen gun.

Second, the glass surface is functionalized with methacrylate groups. 3- (trimethoxysilyl)propyl methacrylate is mixed in ethanol with a concentration of 20% by volume. The pH of the solution is adjusted with acetic acid (Sigma Aldrich) to pH 5. Several drops of the mixed 3-(trimethoxysilyl)propyl methacrylate solution are placed on the glass surface. A second clean glass slide is used to cover the glass slide with the mixed solution in-between. After 30 min, new drops are added to the glass slide and is covered again. After another 30 min, all glass slides are washed with acetone and dried with a nitrogen gun.

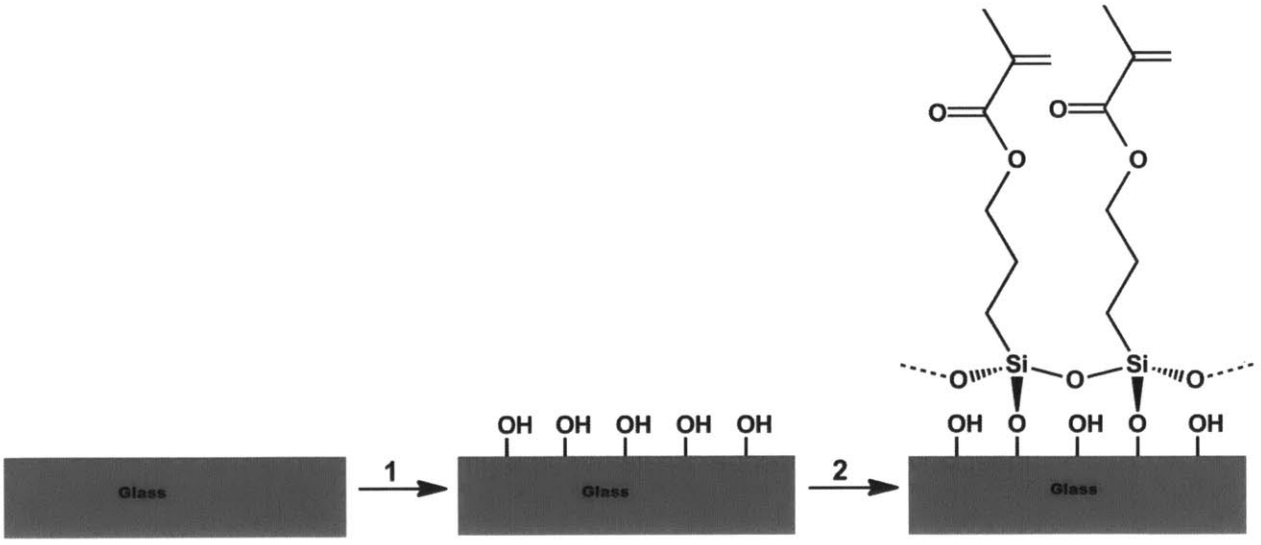

Fig. 4.3 Chemistry of the glass surface treatment process

Chapter 5. Physical Model to Predict Bacterial Population Dynamics in the Microfluidic Cell Culture Chamber

5.1 Introduction

In Chapter 2, we discussed the general design principle how bacteria can be cultured with physical isolation when inter-species chemical communication is retained. In this chapter, we develop physical models to predict bacterial population dynamics during culture under different scenarios, especially different inter-species relationships. Predictions from the physical model can be contrasted with experimental data to infer physiological parameters for bacterial growth or even inter-species relationships. Symbiosis will be the focus of the physical model in this chapter. However, the model can be generalized to other inter-species relationships such as quorum sensing, inhibition, and cheating.

Two physical models are developed in this chapter, one continuum model[45] and an individual-based model[46, 47, 48]. Continuum model assumes population density is a continuous parameter and are usually more rapid to solve and less noisy. Individual-based models track bacteria one by one, thus consuming relatively more computation resources.

Fig. 5.1 shows the field for simulation. Bacteria are seeded into the blue part in the field. The green part simulates ideal nanoporous walls, which do not allow bacteria to cross but allows nutrients or chemicals to diffuse across.

Fig. 5.2 shows the general logic in formulating the physical model[48, 49]. Two regions of simulations are done in an alternate method. The environment simulates the dynamics of chemical distribution in the field. The bacterial region simulates the nutrient update and bacterial growth. All bacteria are assumed to uptake nutrient with a diffusion model (explained in the next section). Every time step, bacteria uptake nutrient and correct the local chemical concentration. Then, changes in local concentration lead to chemical diffusion and redistribution of the nutrient.

In individual-based models, every bacterium is assumed to experience Brownian motion. Only nutrients immediate to the bacteria's position are taken up.

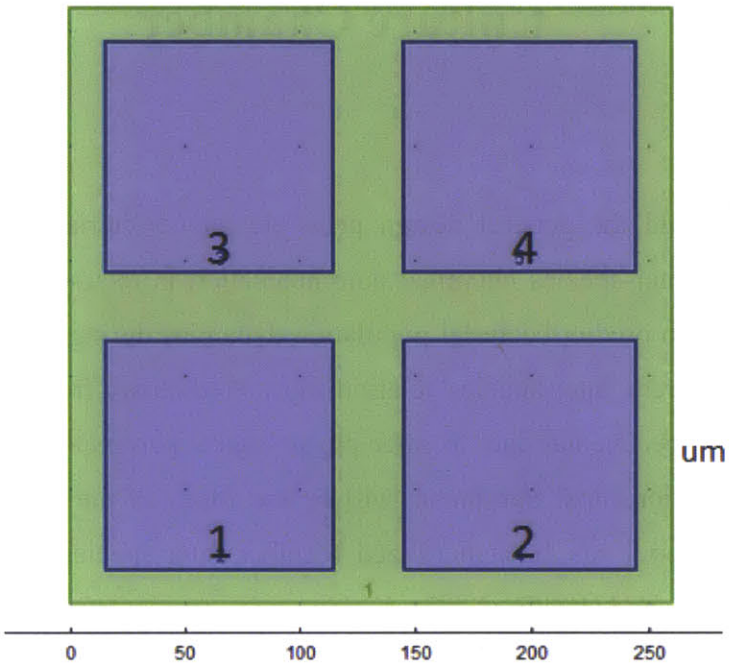

Fig. 5.1 Field for simulation of the physical model

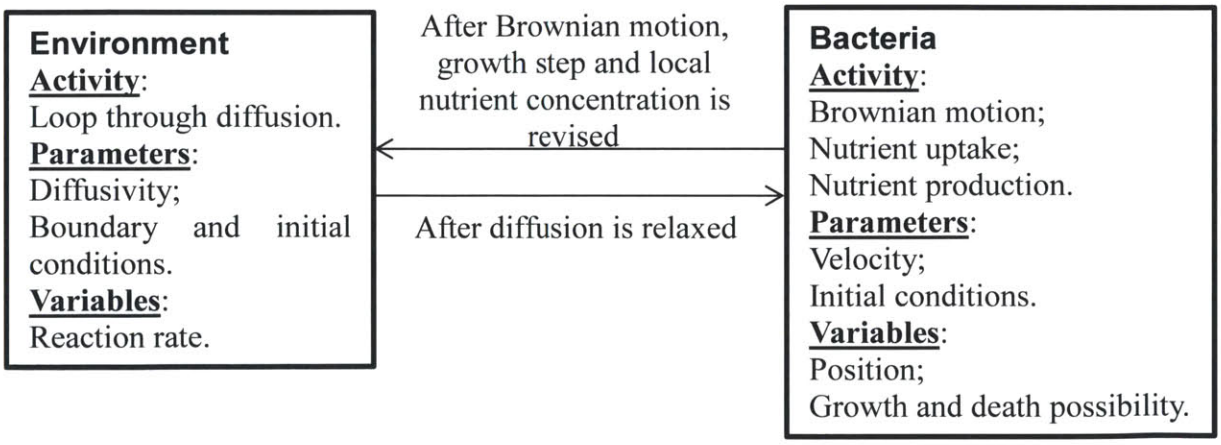

Fig. 5.2 General logic in formulating the physical model

5.2 Continuum Model (CM)

In the Continuum Model (CM), bacteria in the isolated wells are assumed to be uniformly distributed. That is, in an individual well, the bacterial population density is defined as the number of bacteria in the well divided by the volume of the well.

For the environment region, dilute nutrient concentration is assumed, and nutrient redistribution happens only through uptake (or production) by bacteria through diffusion. Thus, nutrient diffusion is governed by the following equation[50]:

$$\frac{\partial c}{\partial t} - D_c \nabla^2 c = R_c \tag{5.1}$$

Where c is the nutrient concentration;

t is the time; and

D_c is the nutrient diffusivity. Diffusivity is assumed to be constant. However, chemical diffusivity in the well is different from diffusivity in the nanoporous walls;

R_c is the rate of nutrient uptake (or production) by bacteria, and is defined in the bacterial region.

For the bacteria, nutrient uptake and population density is defined.

In this model, the nutrient uptake rate is assumed to vary linearly with the bacterial population density, as shown in Equation 5.2[50].

$$R_c = -4\pi a D_c c p \tag{5.2}$$

Where a is the diameter of bacteria.

This nutrient uptake rate is derived with the following three assumptions:

- Bacteria are spherical with diameter of a;
- Nutrient or chemical is uniformly distributed in the field far away from the bacterium;
- Bacteria are not in motion;
- All nutrients on the boundary of the bacterium is taken up;
- Equilibrium state is quickly reached.

Under the above assumptions, Fig. 5.3 shows the nutrient concentration distribution outside of the bacterium. By integrating the flux into the bacterium, we can get the nutrient uptake rate as shown in Equation 5.2.

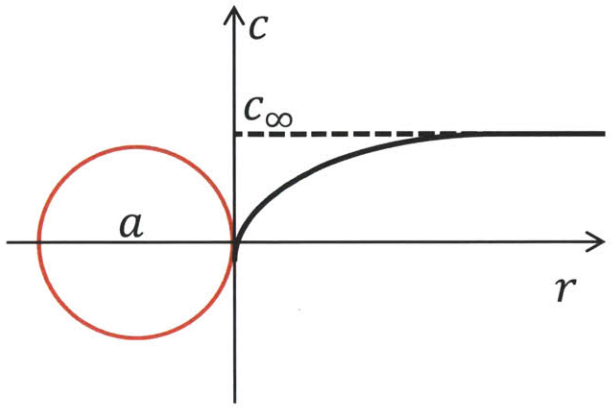

Fig. 5.3 Nutrient concentration distribution outside of the bacterium

The change rate of population density is assumed to be related with net individual growth rate, and current population density. Net individual growth rate takes into account of bacterial growth and death, with the bacterial growth rate assumed to be linear with the nutrient availability. Higher current population density leads to higher population growth rate if nutrient is available. In addition to nutrients, population is limited by availability of physical space.

Overall, the population density dynamics is captured with the following governing equations[50]:

$$\frac{\partial p}{\partial t} = R_p = \left(\mu \frac{c}{c_0} - d\right) \times p \times \left(1 - \frac{p}{K}\right) \tag{5.3}$$

Where R_p is rate of change of population density; and

μ is the individual growth rate when concentration equals c_0. Individual growth rate is assumed to be linear to the nutrient availability;

d is the death rate. Death rate is assumed to constant, regardless of nutrient availability;

K is the carrying capacity of the environment. K is calculated by dividing the total available physical space in the well by the volumetric size of an individual bacterium.

Equations 5.1 to 5.3 are the combined governing equations for the continuum model and the model can be simulated with finite element analysis in the software Comsol Multiphysics (Burlington, MA).

5.3 Individual-Based Model (IBM)

In the Individual-Based Model (IBM), every bacterium is treated to be an independent entity. Every bacterium experiences Brownian motion[51, 52]. In this model, chemotaxis of bacteria is not accounted for as the total physical space (the size of the well) for bacterial motion is quite small. Inside the same well, inter-cellular influence is neglected except for competition for nutrients.

For the environment region, the governing equation remains the same as in the continuum model as Equation 5.1.

For the bacterial region, bacteria are assumed to have a constant swimming speed v. At every time step, a probably test is done to simulate whether bacteria are swimming and in which direction.

The nutrient uptake rate is the discretized form of Equation 5.2:

$$\Delta c = -4\pi a D_c c \Delta t \tag{5.3}$$

Where Δc is the nutrient taken up by bacteria; and

Δt is the time step.

However, as bacteria are swimming, nutrient uptake happens along the trace rather than at a single point as in the continuum model. Therefore, during simulation, nutrient or chemical concentration along the bacterial swimming trace is updated.

The rate of change in population in the IBM is different from that in the CM in that in the IBM, individual bacterium is judged whether they will grow, die or remain. The probability of growth or death is assumed to be a random effect and the probability is discretized from Equation 5.3.

$$\begin{cases} P_g = \left[\mu\frac{c}{c_0} - \frac{p}{K}\left(\mu\frac{c}{c_0} - d\right)\right]\Delta t \approx \mu\frac{c}{c_0} \times \Delta t & (5.4) \\ P_d = d \times \Delta t & (5.5) \end{cases}$$

Where P_g is growth probability of an individual bacterium at every time step;

P_d is the death probability of an individual bacterium at every time step.

During simulation of the IBM, random numbers are generated and compared with P_g and P_d to determine whether an individual bacterium will grow, die or remain.

As the IBM takes more computation resources than the CM, only simulation during the initial stage of bacterial growth is done with the IBM. That is, only when the number of bacteria is quite small compared with the carrying capacity of the well is simulated with the IBM.

5.4 Simulation Results and Discussion

Three circumstances have been simulated to predict population dynamics in the specified field of micro-well arrays. In the first case, population change in a single isolated well is simulated, where bacteria have no other communication with the outside environment or other species except for nutrient competition. In this case, bacteria compete with each other for nutrients. In the second simulation, two species reside in neighboring wells and communicate with each other in a syntrophic way. In this case, how symbiosis contributes to each other's growth is simulated. In the final simulation, the distribution how each species is seeded is revised, where there were more wells occupied by one species than that occupied by the other. In this case, how the physical occupancy of each species influence the abundance of the community is studied.

The field for simulation is shown as Fig. 5.1. Bacteria are seeded into the blue region or inside the well. The seeded number of bacteria is the initial condition for the simulation.

Figure 5.4 shows the simulation results of population change from CM. From figure 5.4, we observe a typical growth pattern of bacteria in a resource-limited environment, where bacteria

experience exponential growth followed by stationary phase and death phase. Experimentally, we found stationary phase lasted longer than the model predicted. The defect in the model lay in the negligence of the fact that bacteria could adjust their own metabolism in a stressed environment. With adjusted metabolism, bacteria need fewer nutrients for survival. Therefore, the model prediction only applies to pre-stationary phase bacterial growth.

Fig. 5.5 shows average population in the well for four simulations from IBM. By comparing Fig. 5.4 and Fig. 5.5 after the first 2000 seconds, both models predict population of about 100 cells in the well. This suggests that the two models are consistent in predicting population dynamics.

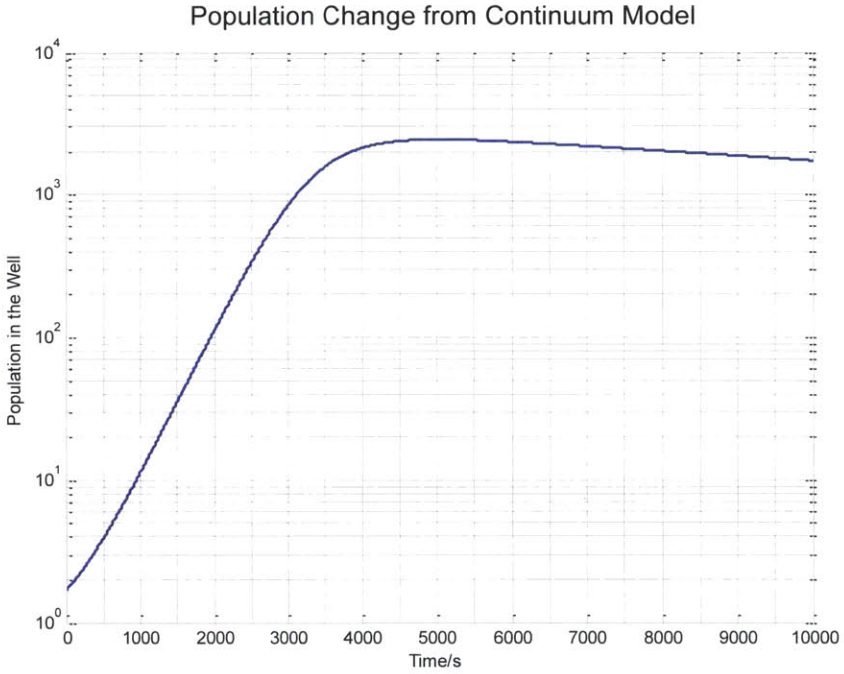

Fig. 5.4 Prediction of population change from the Continuum Model when there is a single strain of bacteria in the Microfluidic Cell Culture Chambers.

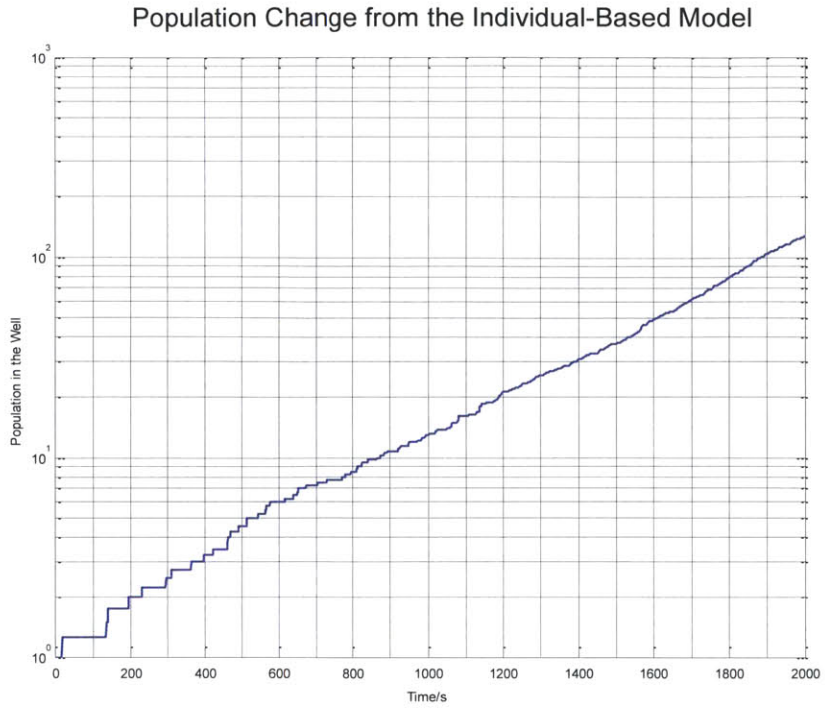

Fig. 5.5 Prediction of population change from the Individual Based Model when there is a single strain of bacteria in the Microfluidic Cell Culture Chambers.

In the second simulation, an imaginary scenario is assumed where two syntrophic species of bacteria are isolated but keep communicating with each other chemically. The physical environment in this case was symmetric for these two species, meaning that the simulation started with exactly the same condition for the two species, except that each species reside in their own chamber. In this simulation, Species 1 in Chamber 1 consumes Chemical A and produces Chemical B; Species 2 in Chamber 2 consumes Chemical B and produces Chemical A. Chemical B will diffuse through the nanoporous wall and benefit Species 2; Chemical A will diffuse through the nanoporous wall and benefit Species 1.

Initially, only one bacterium is seeded in each chamber. There are both Chemical A and Chemical B available in each chamber to boost growth of Species 1 and Species 2. However, these initial nutrients will soon be depleted and both species will have to rely on the other for these nutrients.

Fig. 5.6 predicts growth of each species based on the CM. In this simulation the two species are assumed to be symmetric. This plotted curve represents both species' growth. In this prediction, two species will develop synergistic symbiosis after consuming all naturally available resources.

Fig. 5.7 predicts bacterial growth in each well from IBM. The number of well corresponds to what is shown in Fig. 5.1. Species 1 resides in Well 2 and 3; Species 2 resides in Well 1 and 4. Sudden jumps in the curve means that there are bacteria dividing. The prediction from the IBM is different from that in CM in at least two points. First, growth of the same species in different chambers can be significantly different, even though they have the same initial and boundary conditions. Second, since the initial seed concentration of bacteria in each well is quite small, only one bacterium in each chamber, it is possible that the bacterium may die before dividing.

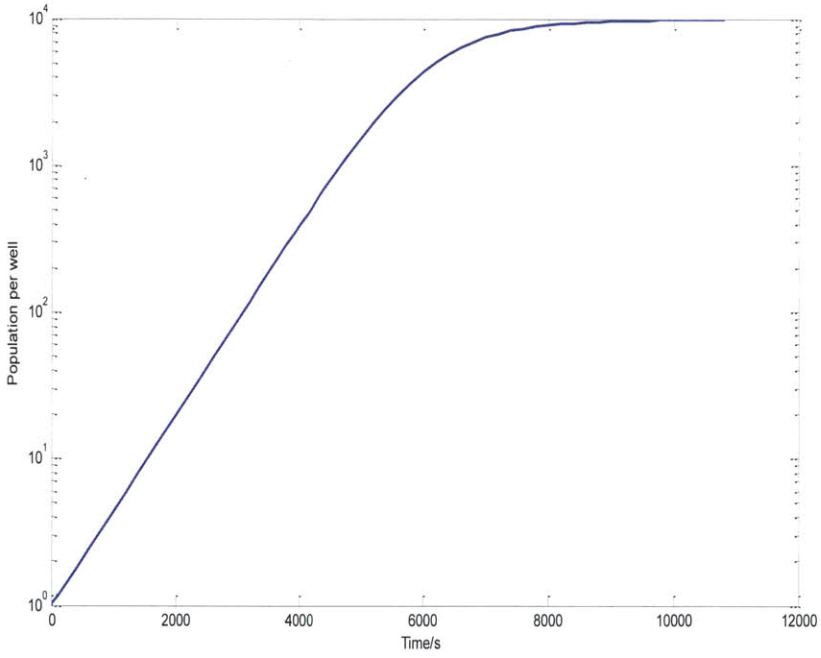

Fig. 5.6 Population change prediction from the CM when two syntrophic strains of bacteria are seeded into the Microfluidic Cell Culture Chambers and are neighbors to each other.

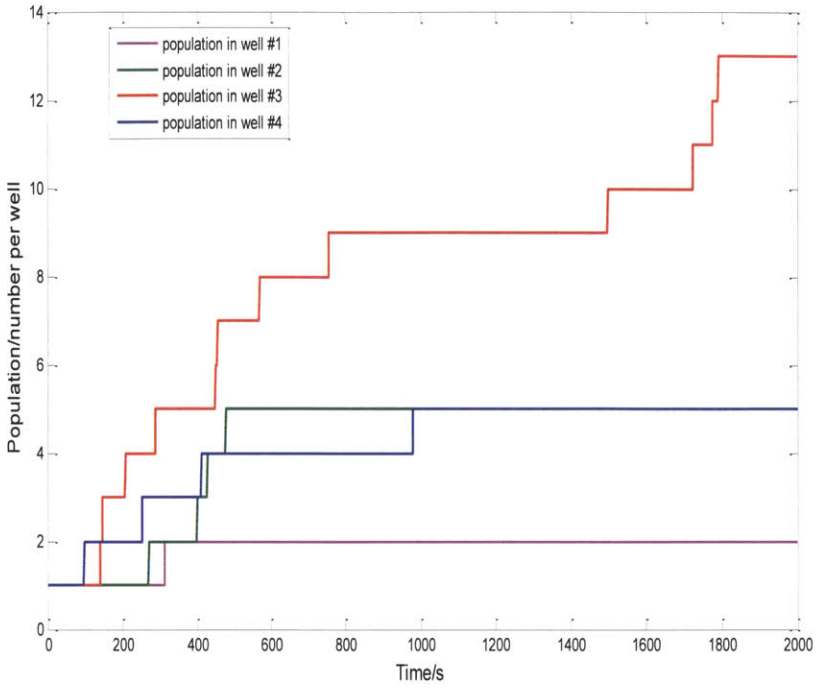

Fig. 5.7 Population change prediction from the IBM when two syntrophic strains of bacteria are seeded into the Microfluidic Cell Culture Chambers and are neighbors to each other.

In the third case, an asymmetric environment is assumed as shown in Fig. 5.8 (previous two simulations use the field of Fig. 5.1). Two syntrophic species were assumed to be seeded in five wells, numbered 1 or 2 in Fig. 5. Species 1 is seeded into type 1 well; Species 2 is seeded into type 2 well. Bacteria in wells A, B, and C will experience different neighboring conditions. For Species 1 residing in Well A, they have Species 2 releasing nutrients that are critical to their survival. Species 2 residing in Well B is very different from Species 2 residing in Well C. The critical nutrients released by Species 1 in Well A will first benefit Species 2 in Well B and then Species 2 in Well C. The symbiosis in this simulation is asymmetric.

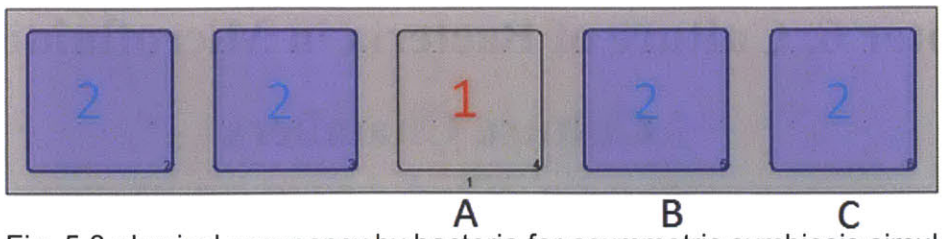

Fig. 5.8 physical occupancy by bacteria for asymmetric symbiosis simulation

Prediction of population change from the CM for the two species in these three types of wells is plotted in Fig. 5.9. Clearly from the figure, we found that the symbiosis was not stable. Populations of each species first increase by consuming the originally available resources. After they have grown to a high population, they have to depend on each other for the critical nutirents, this is because growth of Species 2 in Well B and C are not fast enough to provide sufficient nutrients for Species 1. Then, after Species 1 starts dying out, Species 1 release decreasing amounts of nutrients that are critical to Species 2's survival, which is followed by Species 2' dying out. Metabolically, they were supposed to sustain each other's growth. They could not reach an equilibrium state because the physical occupancy of each species is out of balance.

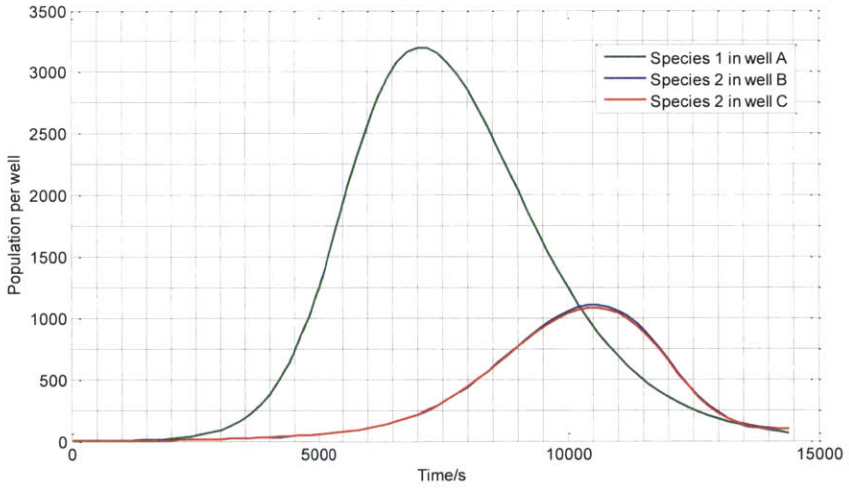

Fig. 5.9 population change prediction for bacteria residing in the three types of wells when two syntrophic strains of bacteria are seeded into the Microfluidic Cell Culture Chambers and occupy unequal amount of space.

Chapter 6. Culture of Bacteria in Microfluidic Cell Culture Chambers

6.1 Introduction

This chapter presents experimental results from culture of different strains of *Escherichia coli* in Microfluidic Cell Culture Chambers based on the design in Chapter 2 and fabrication process in Chapter 4. In the first set of experiments, a single strain of *E. coli* is seeded into the Microfluidic Cell Culture Chambers and the entire growth process is recorded. In the next set of experiments, a pair of syntrophic *E. coli* strains is stochastically seeded into the Microfluidic Cell Culture Chambers and their synergistic growth is studied.

6.2 Cell Seeding Protocol

E. coli are stochastically seeded into the Microfluidic Cell Culture Chambers. The protocol is described in Fig. 6.1. Before the protocol is initiated, *E. coli* is cultured to stationary phase and then diluted to about 1 million cells per milliliter. In the case of co-culture, diluted bacterial solution is mixed before the protocol is started.

In the protocol, a drop of the cell solution is pipetted on top of the HEMA-EDMA micro-well arrays. After 3 minutes, a PDMS cap is applied to seal the micro-well arrays. PDMS is used because it is permeable to oxygen, and oxygen is necessary for *E. coli*'s growth. The trough in the PDMS cap is made to be the same height as the micro-well arrays. The HEMA-EDMA hydrogel swells in contact with water. Therefore, although there is no covalent bonding between HEMA-EDMA and PDMS to secure the sealing, the swelling of HEMA-EDMA leads to a compression force between the cap and the HEMA-EDMA micro-well arrays and contributes to good sealing.

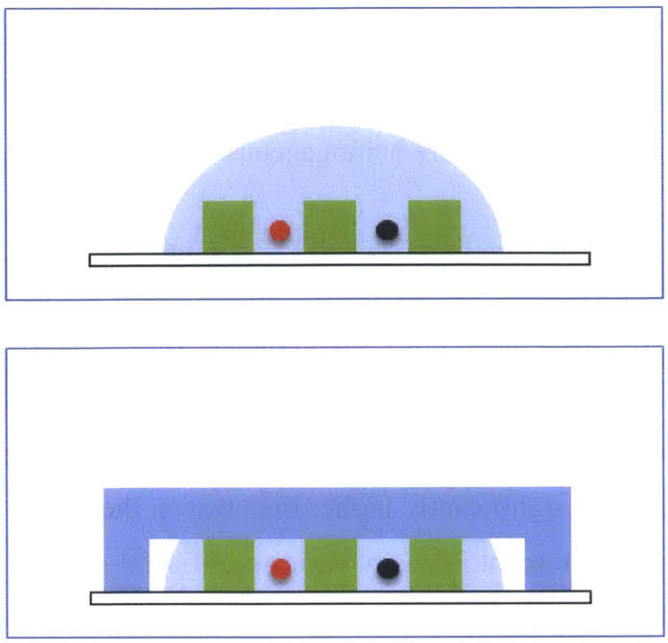

Fig. 6.1 Protocol for seeding bacteria into the Microfluidic Cell Culture Chambers

6.3 Single Strain *E. coli* Culture

In this section, a strain of green fluorescent *E. coli* is seeded into the Microfluidic Cell Culture Chambers, and their growth is filmed with fluorescent microscopy. The purpose of single-strain culture is to validate that the device is capable of physically isolating bacteria, and the material, HEMA-EDMA, is biocompatible.

Fig. 6.2 gives two snapshots of a video of one bacterium inside a chamber immediately after the bacteria are seeded into the device. The bacterium is swimming inside the chamber, moving back and forth within the nanoporous HEMA-EDMA walls. This demonstrates that the hydrogel is capable of isolating bacteria physically.

Fig. 6.3 consist of snapshots of the single-strain *E. coli* culture process. The three images are taken immediately after bacteria are seeded (Fig. 6.3a), after about six hours of' culture (Fig. 6.3b), and after roughly 12 hours (Fig. 6.3c). In Fig. 6.3a, we observe a stochastic distribution of bacteria among the chambers. The number of bacteria inside a chamber ranges from zero to six in this image. The results after about 12 hours' culture show that the growth of *E. coli* is highly

heterogeneous. Moreover, we notice that there are still chambers that are unoccupied by any bacteria. These two results indicate that bacteria did not jump from chamber to chamber, because otherwise the culture results would be more homogeneous.

Comparing Fig. 6.3a and Fig. 6.3c, we see that the final growth condition is not simply a function of initial seeding bacterial concentration. In the initial seeding result, the chamber circled in black (second row from the bottom, sixth column from the left) is the highest bacterial concentration among all chambers. The chamber circled in red (sixth row from the bottom, sixth from the left) contains only two bacteria. However, after about 12 hours' culture, fluorescent intensity in the red chamber is significantly higher than that in the black chamber. It should be pointed out that individual fluorescent intensity varies significantly. Higher fluorescent intensity does not necessarily indicate higher population. However, in Fig. 6.3c, it is clearly shown that bacteria have filled almost the whole space of the red chamber, while bacteria in the black chamber are still sparsely distributed. This is solid proof that bacterial concentration in the red chamber is higher than that in the black chamber.

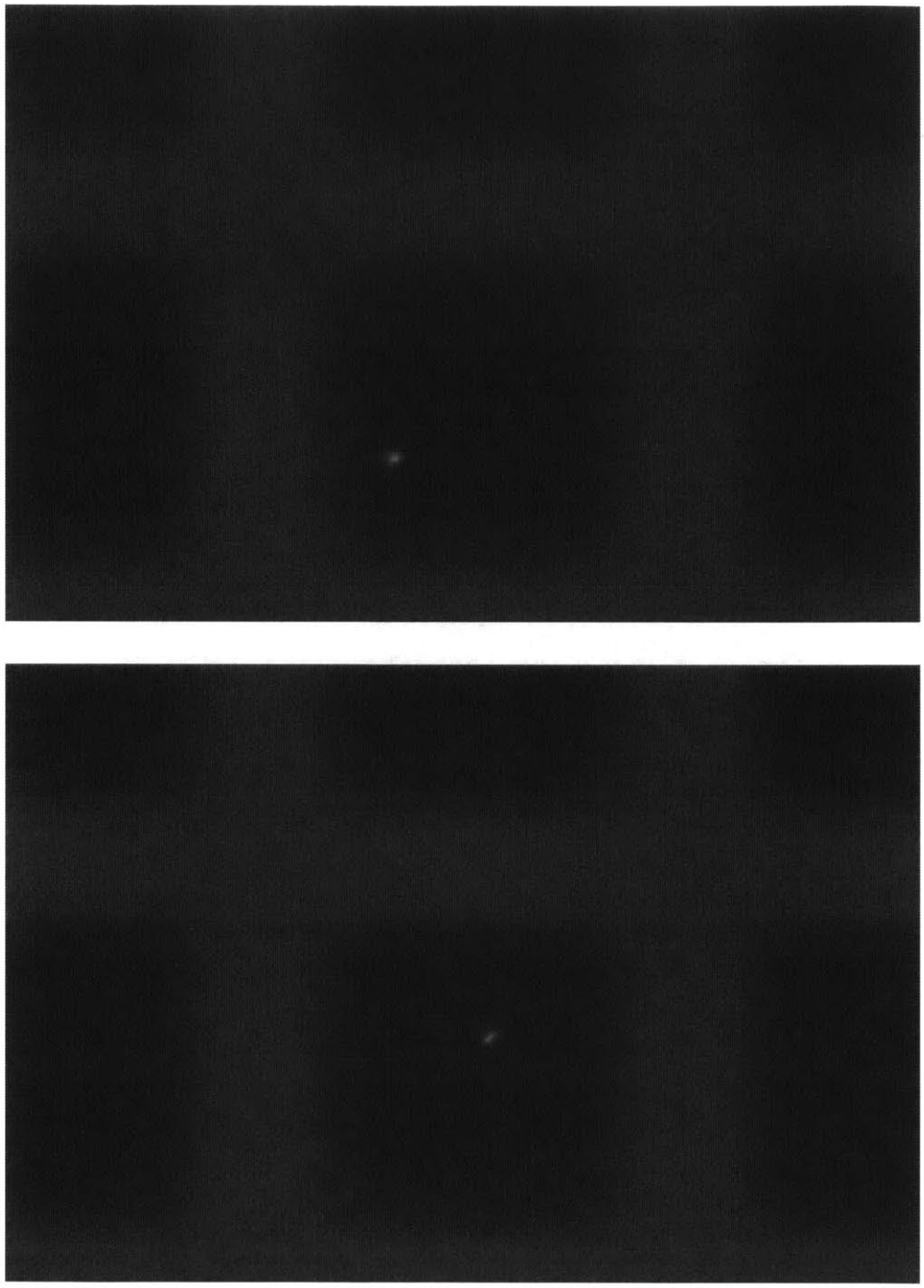

Fig. 6.2 Two snapshots from a video of one bacterium inside a chamber immediately after the bacteria are seeded into the device

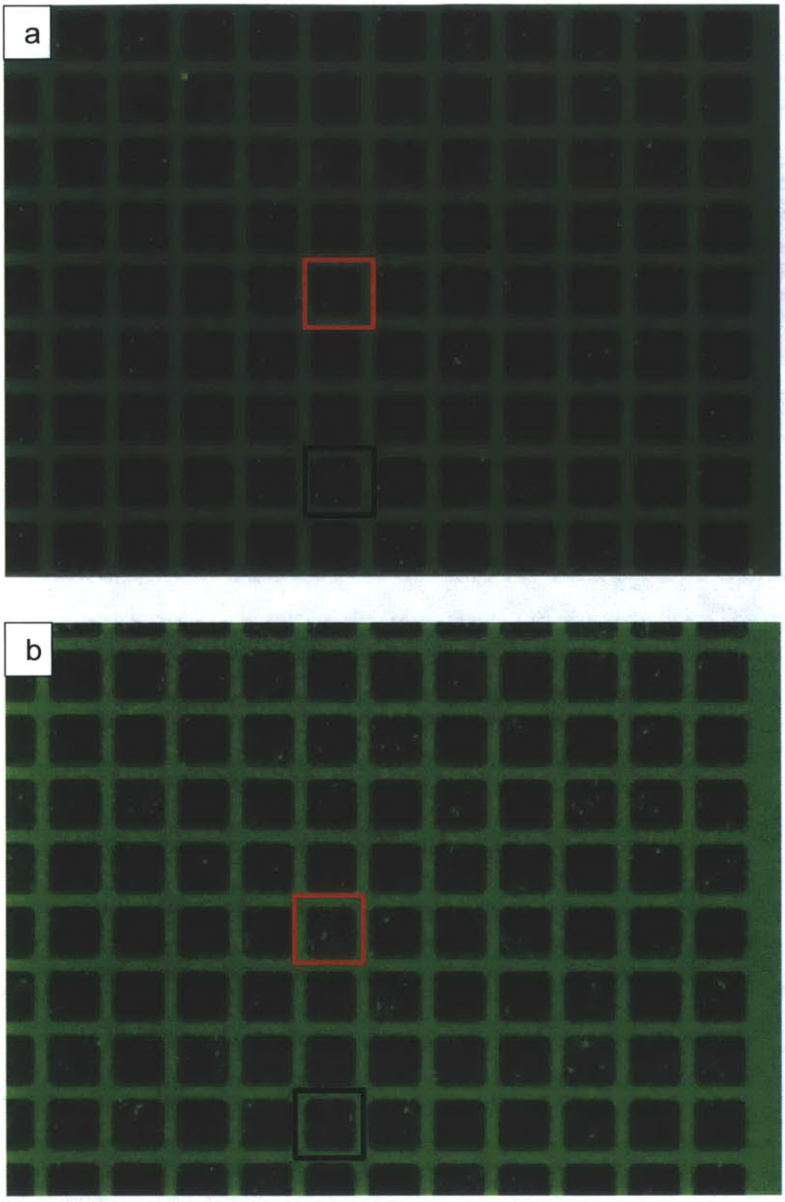
a
b

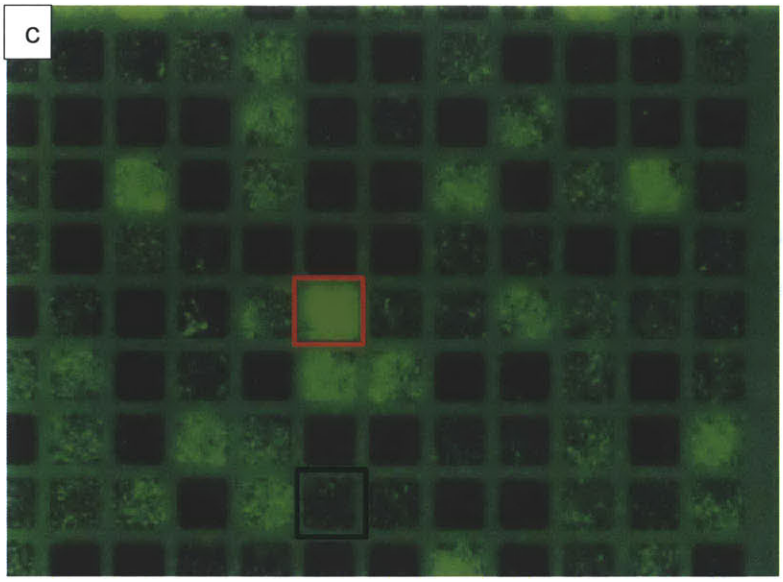

Fig. 6.3 Images of the single-strain *E. coli* culture process. a) Immediately after the bacteria are seeded; b) After about six hours' culture; c) After about 12 hours' culture.

6.4 Construction of a Syntrophic Pair of *E. coli*

A syntrophic pair of *E. coli* is constructed from auxotrophic *E. coli* from the Keio collection[53, 54]. The selected strains of auxotrophic *E. coli* are genetic knockout strains from wild type *E. coli*, primarily from *E. coli K-12*. In each strain of auxotrophic *E. coli*, some portion of genetic information is deleted. Metabolically, each auxotrophic strain is unable to synthesize at least an essential metabolite and thus has to depend on external supply of that metabolite.

The four pairs of auxotrophic *E. coli* selected are Δ*trp*, Δ*tyr*, Δ*cys*, and Δ*arg*:

- Δ*trp*: unable to synthesize tryptophan;
- Δ*tyr*: unable to synthesize tyrosine;
- Δ*cys*: unable to synthesize cysteine;
- Δ*arg*: unable to synthesize arginine.

As shown above, each auxotrophic *E. coli* is unable to synthesize one particular kind of amino acid, and therefore they are unable to grow alone in M9 minimal media. However, when any two of those species are cultured together in M9 minimal media, synergistic growth may develop

because each of them can synthesize the amino acid that the other strain need and the whole community can develop by sharing resources.

To differentiate bacteria, every strain is transformed to constitutively encode either green fluorescent proteins (GFP) or red fluorescent proteins (RFP). Thus, under fluorescence microscopy, each strain can be differentiated.

Table 6.1 shows the experimental results of two-strain co-culture in culture tubes. R3+G3 and R4+G4 are control groups. Both control groups show limited or no growth, which is a proof that the *E. coli* strain is not contaminated. All other mixed culture shows synergistic growth. However, under fluorescence microscopy, it is observed that only R4+G3 culture shows significant growth of both red and green bacteria. In all other mixed culture, red bacteria benefit more than green bacteria from the mixed culture. Therefore, the R4 and G3 pair is selected for co-culture in the microfluidic device.

Table 6.1 Experimental results of two-strain co-culture in culture tubes

	Day 1 OD_{600}	Day 2 OD_{600}	Day 3 OD_{600}	Day 4 OD_{600}
R3+G1	0.021	0.033	0.110	0.233
R3+G2	0.014	0.018	0.098	0.879
R3+G3	0.010	0.027	0.024	0.015
R3+G4	0.013	0.027	0.155	0.632
R4+G1	0.023	0.070	0.147	0.243
R4+G2	0.016	0.029	0.077	0.529
R4+G3	0.014	0.100	0.482	0.596
R4+G4	0.017	0.019	0.016	0.010

Note: R, G denote red and green fluorescent, respectively;
1, 2, 3,4 stands for Δtrp, Δtyr, Δcys, and Δarg respectively.

6.5 Co-Culture in the Microfluidic Cell Culture Chambers

The protocol for co-culture of R4 (Δ*arg*, red fluorescent) and G3 (Δ*cys*, green fluorescent) is shown in Fig. 6.4. First, auxotrophic *E. coli* is grown on LB broth alone. Auxotrophic *E. coli* can grow on LB broth as LB broth provides all kinds of amino acids for the survival and growth of auxotrophic *E. coli*. Second, after auxotrophic *E. coli* reach stationary phase, the bacterial solution is diluted by 100 times and cultured in M9 minimal media overnight to consume all remaining critical amino acids. Third, cell solution from M9 minimal media is mixed and diluted by 100 times before seeding into the microfluidic device.

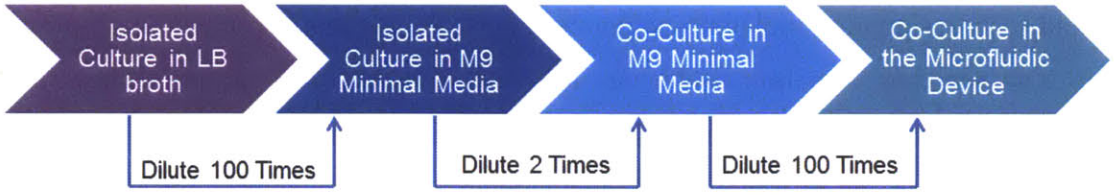

Fig. 6.4 Protocol for co-culture of *E.coli* Δ*arg* and Δ*cys*

To this stage, co-culture in the microfluidic device has not shown significant growth of both strains. Several possible reasons are proposed for further investigations. From the perspective of the device, evaporation may happen inside the microfluidic device, which indirectly increases chemical concentration inside the chambers. This can be negative for bacterial growth. From the biological perspective, auxotrophic strains used in this experiment are sharing resources that are critical to themselves. For example, in the co-culture of R4+G3, R4 is sharing with G3 cysteine, which the latter is unable to synthesize. However, R4 needs cysteine for its survival. It can happen that in the microfluidic environment, auxotrophic strains have changed their strategy to not share resources. It is also possible that R4 and G3 did grow synergistically, but fluorescent proteins are not expressed. It has been observed that bacteria may restrain unnecessary expression of some proteins under high stress conditions.

Chapter 7. Future Work and Conclusion

7.1 Future Work

Quorum sensing strains are proposed to be co-cultured in the device to first study inter-species communication in order to further investigate how bacteria communicate in the Microfluidic Cell Culture Chambers.

Quorum sensing[55] is mechanism which bacteria use to coordinate gene expression according to population density, schematically shown in Fig. 7.1. Sender strains of quorum sensing can produce and secrete signaling molecules when they sense the population density is above a given threshold. The secreted signaling molecules are sensed by receiver strains. After receiving signaling molecules, receiver strains restrain gene expression and thus reduce population growth rate. The receiver strain can be transformed to encode green fluorescent proteins after sensing the quorum sensing molecules. In this way, we can observe with fluorescence microscopy that inter-species chemical communication is occuring. The sender strain and the receiver strain can be the same strain, or they can be different strains. When sender strain and receiver strain are different strains, we can use them to study inter-species chemical communication.

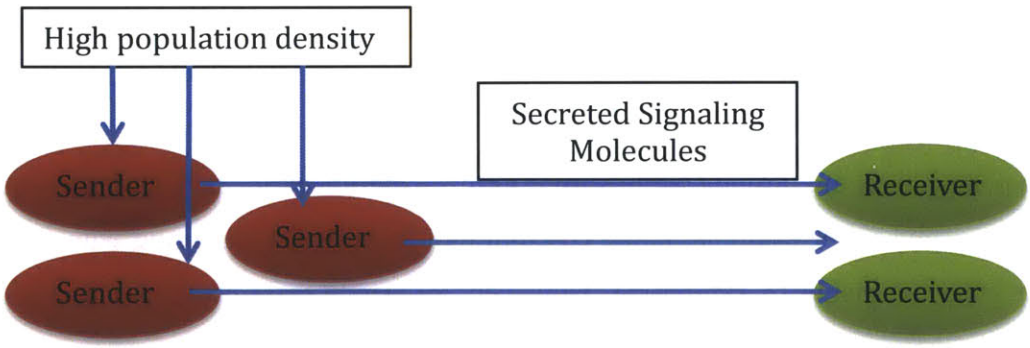

Fig. 7.1 Working principle of quorum sensing pairs

The advantages using quorum sensing strains are two-fold. First, in quorum sensing, the signaling molecule can be a small molecule. For example, in *E. coli*'s quorum sensing, the involved signaling molecule can be autoinducer-2 (AI-2). The molecular formula for AI-2 is

$C_5H_{10}BO_7$. In chapter 3, we have experimentally validated that the nanoporous membrane is capable of allowing small molecules, like AI-2, to pass through.

Second, quorum sensing strains do not depend on each other for initial growth. As explained in Chapter 6.5, auxotrophic pairs may change their strategies in nutrient lean environment. In contrast, during the initial growth stage, quorum sensing pairs grow independently, just like pure culture *E. coli* in the Microfluidic Cell Culture Chambers. After the sensor strain in the quorum sensing pair grow to sufficiently high population density, they will start synthesizing and secreting signaling molecules. These secreted signaling molecules can be received by the receiver strain after diffusing across the nanoporous membrane.

By using the quorum sensing strains, we can study inter-species interactions without worrying about any bacterial metabolic strategy changes confounding the results.

7.2 Conclusions

In this work, we developed a microfluidic device for co-culturing physically isolated bacteria, while retaining their chemical communication. The device is fabricated with replica molding process with glass as the substrate. We are capable of observing bacterial growth inside this custom made microfluidic device.

We used the hydrogel HEMA-EDMA in building the microfluidic device. HEMA-EDMA is characterized for its porous structure using Environmental SEM. Chemical diffusivity through HEMA-EDMA membrane is characterized with a customized dual-chamber diffusion cell. By changing the solvent ratio in cross-linking HEMA-EDMA, we can obtain HEMA-EDMA of different pore sizes, which means affects the diffusivity for chemicals.

In our physical model for predicting population change in the Microfluidic Cell Culture Chambers we analyzed three scenarios: pure competition, symmetric symbiosis and asymmetric symbiosis. We identified the influence of bacterial chamber occupancy on the abundance of the community.

We have successfully cultured single-strain *E. coli* with the device and demonstrated that *E. coli* can be physically isolated during growth with the HEMA-EDMA walls. This also proves that HEMA-EDMA is compatible with *E. coli*'s growth.

Lastly, we developed a protocol for co-culturing communicating bacteria. Our future work will incorporate quorum sensing strains to look into inter-species chemical communication.

Appendix A

Matlab Code for the Individual-Based Model

- **Main code:**

```
C1(:,:,1)=c0*ones(rows, columns);          % nutrient 1 concentration field initialization.
Nutrient 1 consumed by Spe1 and produced by Spe2.

C2(:,:,1)=c0*ones(rows, columns);          % nutrient 2 concentration field initialization.
Nutrient 2 consumed by Spe2 and produced by Spe1.

Spe1Arr=Bacteria(xInitSpe1,yInitSpe1);    % storing species 1

Spe2Arr=Bacteria(xInitSpe2,yInitSpe2);    % storing species 2

Spe3Arr=Bacteria(xInitSpe3,yInitSpe3);    % storing species 3

Spe4Arr=Bacteria(xInitSpe4,yInitSpe4);    % storing species 4

Spe1Num=1;

Spe2Num=1;

Spe3Num=1;

Spe4Num=1;

Spe1Pop=zeros(1,TotalTimeSteps);

Spe2Pop=zeros(1,TotalTimeSteps);

Spe3Pop=zeros(1,TotalTimeSteps);

Spe4Pop=zeros(1,TotalTimeSteps);

Spe1Pop(1)=Spe1Num;

Spe2Pop(1)=Spe2Num;

Spe3Pop(1)=Spe3Num;

Spe4Pop(1)=Spe4Num;


for t=2:TotalTimeSteps
```

```
fprintf('This is timestep %d.\n',t)
Spe1Pop(t)=Spe1Num;                % record population at time t
Spe2Pop(t)=Spe2Num;
Spe3Pop(t)=Spe3Num;
Spe4Pop(t)=Spe4Num;

C1=Diff(C1,t-1,D,k,h,columns,rows);          % recall diffusion of nutrient 1
C2=Diff(C2,t-1,D,k,h,columns,rows);          % recall diffusion of nutrient 2
  for Index=1:Spe1Num
    if(Spe1Arr(Index).alive==1)   % only alive bacteria go through the following calculation
      xPos=Spe1Arr(Index).xLoc;
      yPos=Spe1Arr(Index).yLoc;
      ScaRat=C1(yPos,xPos,t)/c0;              % scaling ratio for calculating growth
probabiliy
      Pg=(mu*ScaRat-(mu*ScaRat-d)*Spe1Num/K);      % growth probability
      Pd=d;                            % death probabiliy
      if(rand(1)<Pg)
        Spe1Num=Spe1Num+1;
        Spe1Arr(Spe1Num)=Bacteria(xPos,yPos);
      end
      if(rand(1)<Pd)
        Spe1Arr(Index).alive=0;
      end
      [Spe1Arr(Index),C1,C2]=Brownian(Spe1Arr(Index),velocity,C1,C2,t);      %
bacterial Brownian motion
    end
```

```
    end
    for Index=1:Spe2Num
      if(Spe2Arr(Index).alive==1)
        xPos=Spe2Arr(Index).xLoc;
        yPos=Spe2Arr(Index).yLoc;
        ScaRat=C2(yPos,xPos,t)/c0;
        Pg=(mu*ScaRat-(mu*ScaRat-d)*Spe2Num/K);
        Pd=d;
        if(rand(1)<Pg)
          Spe2Num=Spe2Num+1;
          Spe2Arr(Spe2Num)=Bacteria(xPos,yPos);
        end
        if(rand(1)<Pd)
          Spe2Arr(Index).alive=0;
        end
        [Spe2Arr(Index),C2,C1]=Brownian(Spe2Arr(Index),velocity,C2,C1,t);
      end
    end
    for Index=1:Spe3Num
      if(Spe3Arr(Index).alive==1)   % only alive bacteria go through the following calculation
        xPos=Spe3Arr(Index).xLoc;
        yPos=Spe3Arr(Index).yLoc;
        ScaRat=C2(yPos,xPos,t)/c0;                % scaling ratio for calculating growth
probabiliy
        Pg=(mu*ScaRat-(mu*ScaRat-d)*Spe3Num/K);        % growth probability
```

```
        Pd=d;                                % death probabiliy
        if(rand(1)<Pg)
          Spe3Num=Spe3Num+1;
          Spe3Arr(Spe3Num)=Bacteria(xPos,yPos);
        end
        if(rand(1)<Pd)
          Spe3Arr(Index).alive=0;
        end
        [Spe3Arr(Index),C2,C1]=Brownian(Spe3Arr(Index),velocity,C2,C1,t);          %
bacterial Brownian motion
      end
    end
    for Index=1:Spe4Num
      if(Spe4Arr(Index).alive==1)   % only alive bacteria go through the following calculation
        xPos=Spe4Arr(Index).xLoc;
        yPos=Spe4Arr(Index).yLoc;
        ScaRat=C1(yPos,xPos,t)/c0;                  % scaling ratio for calculating growth
probabiliy
        Pg=(mu*ScaRat-(mu*ScaRat-d)*Spe4Num/K);          % growth probability
        Pd=d;                                % death probabiliy
        if(rand(1)<Pg)
          Spe4Num=Spe4Num+1;
          Spe4Arr(Spe4Num)=Bacteria(xPos,yPos);
        end
        if(rand(1)<Pd)
          Spe4Arr(Index).alive=0;
```

```
            end
            [Spe4Arr(Index),C2,C1]=Brownian(Spe4Arr(Index),velocity,C2,C1,t);          %
bacterial Brownian motion
          end
        end
end
```

- **Class Bacteria:**

```
classdef Bacteria
  %define class of Bacteria
  %live==1 means the bacteria is alive, else it's dead.

  properties
    alive=1;
    xLoc;
    yLoc;
  end
  methods
    function obj=Bacteria(x,y)
      obj.xLoc=x;
      obj.yLoc=y;
    end
  end
  end
```

- **Bacterial Brownian Motion:**

```
function [Bacteria,Cin,Cout] = Brownian(Bacteria,velocity,Cin,Cout,t)
%UNTITLED3 Summary of this function goes here
%   Detailed explanation goes here
xInit=Bacteria.xLoc;
yInit=Bacteria.yLoc;
% x-direction Brownian motion
if(rand(1)>1/2)
   Bacteria.xLoc=Bacteria.xLoc+velocity;
else Bacteria.xLoc=Bacteria.xLoc-velocity;
end

% y-direction Brownian motion
if(rand(1)>1/2)
   Bacteria.yLoc=Bacteria.yLoc+velocity;
else Bacteria.yLoc=Bacteria.yLoc-velocity;
end

if(Bacteria.xLoc<16)
   Bacteria.xLoc=16;
end
if(Bacteria.xLoc>245)
   Bacteria.xLoc=245;
end
if(Bacteria.xLoc>115&&Bacteria.xLoc<130)
```

```
   Bacteria.xLoc=115;
end
if(Bacteria.xLoc>130&&Bacteria.xLoc<146)
   Bacteria.xLoc=146;
end
if(Bacteria.yLoc<16)
   Bacteria.yLoc=16;
end
if(Bacteria.yLoc>245)
   Bacteria.yLoc=245;
end
if(Bacteria.yLoc>115&&Bacteria.yLoc<130)
   Bacteria.yLoc=115;
end
if(Bacteria.yLoc>130&&Bacteria.yLoc<146)
   Bacteria.yLoc=146;
end



%nutrint uptake and production
if(xInit<Bacteria.xLoc)
   slope=(Bacteria.yLoc-yInit)/(Bacteria.xLoc-xInit);
   for x=xInit:Bacteria.xLoc
      y=floor(yInit+slope*(x-xInit));
      Cin(x-1:x+1,y-1:y+1,t)=Cin(x-1:x+1,y-1:y+1,t)/2;
```

```
        Cin(x,y,t)=0;
        Cout(x-1:x+1,y-1:y+1,t)=0.1+Cout(x-1:x+1,y-1:y+1,t)/2;
        Cout(x,y,t)=0.2;
    end
end
if (xInit>Bacteria.xLoc)
        slope=(Bacteria.yLoc-yInit)/(Bacteria.xLoc-xInit);
    for x=Bacteria.xLoc:xInit
        y=floor(yInit+slope*(x-xInit));
        Cin(x-1:x+1,y-1:y+1,t)=Cin(x-1:x+1,y-1:y+1,t)/2;
        Cin(x,y,t)=0;
        Cout(x-1:x+1,y-1:y+1,t)=0.1+Cout(x-1:x+1,y-1:y+1,t)/2;
        Cout(x,y,t)=0.2;
    end
end
if (xInit==Bacteria.xLoc)
    x=xInit;
    for y=yInit:Bacteria.yLoc
        Cin(x-1:x+1,y-1:y+1,t)=Cin(x-1:x+1,y-1:y+1,t)/2;
        Cin(x,y,t)=0;
        Cout(x-1:x+1,y-1:y+1,t)=0.1+Cout(x-1:x+1,y-1:y+1,t)/2;
        Cout(x,y,t)=0.2;
    end
end
```

```
end
```

- **Concentration Update**

```
function C = Diff(C,t,D,k,h,columns,rows)
%An explict way of calculating the concentration field at t=t+1;

%concentration due to diffusion;
for i=2:rows-1
   for j=2:columns-1
      C(i,j,t+1)=C(i,j,t)+k*D/h^2*(C(i-1,j,t)+C(i+1,j,t)+C(i,j-1,t)+C(i,j+1,t)-4*C(i,j,t));
   end
end

% Symmetry boundary conditions
  C(1,:,t+1)=C(2,:,t);
  C(rows,:,t+1)=C(rows-1,:,t);
  C(:,1,t+1)=C(:,2,t);
  C(:,columns,t+1)=C(:,columns-1,t);
end
```

- **Movie driver**

```
figure('vis','off') %setting off displaying the figures

fdirout='C2'; %route of image series to be saved; the route need to be created first in the
directory;
```

```
fbaseout='movie';          %image name;
for t=1:TotalTimeSteps
pcolor(C2(:,:,t))              % 2D mesh plot
axis equal                  % setting display scale of x and y axes equal
axis ([1 columns 1 rows])          % axis ([xmin xmax ymin ymax])
caxis([0 0.2])               % in order to have the same color bar
shading flat                % setting off the grid of the pcolor
shading interp               % create a smooth image
colorbar                    % display colorbar at the side
filename=[fdirout,'\',fbaseout,int2str(t),'.jpg'];
print('-djpeg',filename);      % -djpeg is required to save the image in the format of jpg
end
```

Bibliography

[1] Pace NR. A Molecular View of Microbial Diversity and the Biosphere. *Science,* 276:734-740, 1997.

[2] Fuhrman JA, McCallum K, & Davis AA. Phylogenetic diversity of marine subsurface microbial communities from the Atlantic and Pacific Oceans. *Applied Environmental Microbiology.* 59(5):1294-1302, 1993.

[3] Amann RI, Ludwig W, and Schleifer KH. Phylogenetic identification and in situ detection of individual microbial cells without cultivation. Microbiological Reviews. 59:143-169, 1995.

[4] Woese CR. Bacterial evolution. *Microbiological Reviews.* 51:221–71, 1987.

[5] Woese CR, Kandler O, Wheelis ML. Towards a natural system of organisms: proposal for the domains Archaea, Bacteria, and Eucarya. *Proceedings of the National Academy of Sciencesof the United States of America.* 87:4576–79, 1990.

[6] Woese CR, Stackebrandt E, Macke TJ, Fox GE. A phylogenetic definition of the major eubacterial taxa. *Systematic and Applied Microbiology.* 6:143–51, 1985.

[7] Rappe MS, Giovannoni SJ. The uncultured microbial majority. *Annual Review of Microbiology.* 57:369–94, 2003.

[8] Curtis TP, Sloan WT, and Scannell JW. Estimating prokaryotic diversity and its limits. *Proceedings of the National Academy of Sciences of the United States of America.* 99:10494–10499, 2002.

[9] Hughes, JB, Hellmann, JJ, Ricketts, TH. and Bohannan, BJ. Counting the uncountable: statistical approaches to estimating microbial diversity. *Applied Environmental Microbiology.* 67:4399–4406, 2001.

[10] Torsvik V, Daae FL, Sandaa RA, and Ovreas L, Novel techniques for analysing microbial diversity in natural and perturbed environments. *Journal of Biotechnology.* 64:53–62, 1998.

[11] Knight V, Sanglier JJ, DiTullio D, Braccili S, Bonner P, Waters J, Hughes D, Zhang L. Diversifying microbial natural products for drug discovery. *Applied Microbiology and Biotechnology.* 62:446–458, 2003.

[12] Keller M, and Zengler K. Tapping into microbial diversity. *Nature Reviews Microbiology.* 2: 141-150, 2004.

[13] Winterberg H. Zur Methodik der Bakterienzahlung. *Zeitschr f Hyg* 29:75–93, 1898.

[14] Staley JT, Konopka A. Measurement of in situ activities of nonphotosynthetic microorganisms in aquatic and terrestrial habitats. *Annual Review of Microbiology.* 39:321–346, 1985.

[15] D'Onofrio A, Crawford JM, Stewart EJ, Witt K, Gavrish E, Epstein S, Clardy J, and Lewis K. Siderophores from Neighboring Organisms Promote the Growth of Uncultured Bacteria. *Chemistry & Biology.* 17(3): 254-264, 2010.

[16] Faust K, Raes J. Microbial interactions: from networks to models. *Nature Reviews Microbiology.* 10: 538-550, 2012.

[17] Lidicker WZA. Clarification of interactions in ecological systems. *Bioscience.* 29: 475–477, 1979.

[18] Agrawal R, Imielinski T, and Swami A. Mining association rules between sets of items in large databases. *ACM SIGMOD Record.* 22:207–216, 1993.

[19] Chaffron S, Rehrauer H, Pernthaler J, and Von Mering C. A global network of coexisting microbes from environmental and whole-genome sequence data. *Genome Research*. 20:947–959, 2010.

[20] Costello EK, Lauber CL, Hamady M, Fierer N, Gordon FI, Knight R. Bacterial community variation in human body habitats across space and time. *Science.* 326:1694–1697, 2009.

[21] Freilich S, Kreimer A, Meilijson I, Gophna U, Sharan R, and Ruppin E. The large-scale organization of the bacterial network of ecological co-occurrence interactions. *Nucleic Acids Research*. 38:3857–3868, 2010.

[22] Freilich S, Zarecki R, Eilam O, Segal ES, Henry CS, Kupiec M, Gophna U, Sharan R, and Ruppin E. Competitive and cooperative metabolic interactions in bacterial communities. *Nature Communications*. 2:589, 2011.

[23] May RM. Biological populations with nonoverlapping generations: stable points, stable cycles, and chaos. *Science.* 186:645–647, 1974.

[24] Becks L, Hilker FM, Malchow H, Jürgens K, and Arndt H. Experimental demonstration of chaos in a microbial food web. *Nature*, 435:1226–1229, 2005.

[25] Straight PD, Kolter R. Interspecies Chemical Communication in Bacterial Development. *Annual Review of Microbiology*. 63:99 - 118, 2009.

[26] Stewart EJ. Growing Unculturable Bacteria. Journal of Bacteriology. 194(16): 4151 - 4160, 2012.

[27] Kaeberlein T, Lewis K, Epstein SS. Isolating "uncultivable" microorganisms in pure culture in a simulated natural environment." *Science.* 296(5570): 1127-1129, 2002.

[28] Nichols D, Cahoon N, Trakhtenberg EM, Pham L, Mehta A, Belanger A, Kanigan T, Lewis K, Epstein SS. Use of Ichip for High-Throughput In Situ Cultivation of "Uncultivable" Microbial Species. *Applied and Environmental Microbiology* 76(8): 2445-2450, 2010.

[29] Zengler KT, Toledo G, Rappé M, Elkins J, Mathur EJ, Short JM, and Keller M. Cultivating the uncultured. *Proceedings of the National Academy of Sciences of the United States of America.* 99(24): 15681–15686, 2002.

[30] Ben-Dov E, Kramarsky-Winter E, and KushMaro A. An in situ method for cultivating microorganisms using a double encapsulation technique. *FEMS Microbiology Ecology.* 68(3): 363-371, 2009.

[31] Ingham CJ, Sprenkels A, Bomer J, Molenaar D, Berg A, Vlieg J, and Vos W. The micro-Petri dish, a million-well growth chip for the culture and high-throughput screening of microorganisms. *Proceedings of the National Academy of Sciences of the United States of America.* 104(46): 18217-18222, 2007.

[32] Yi C, Tsao CY, Wu HC, Luo X, Terrell JL, Betz J, Payne GF, Bentley WE, and Rublof GW. Electroaddressing Functionalized Polysaccharides as Model Biofilms for Interrogating Cell Signaling. *Advanced Functional Materials*. 22:519-528, 2011.

[33] Xia Y, Whitesides GM. Soft Lithography. *Annual Review of Materials Research.* 28:153–184. 1998

[34] Whitesides GM, Ostuni E, Takayama S, Jiang X, and Ingber DE. Soft lithography in biology and biochemistry. Annual Review of Biomedical Engineering. 3:335-373, 2001.

[35] Wichterle O, Lim D, Hydrophilic gels in biologic use, *Nature.* 185:117-118, 1960.

[36] Hoffman A. Hydrogels for biomedical applications. *Advanced Drug Delivery Reviews*. 64: 18-23, 2012.

[37] Seliktar D. Designing cell-compatible hydrogels for biomedical applications. *Science*. 336:1124-1128, 2012.

[38] Nicolson PC, Vogt J. Soft contact lens polymer: an evolution. *Biomaterials*. 22(24):3273-3283, 2001.

[39] Langer R, Peppas NA. Advances in Biomaterials, Drug Delivery, and Bionanotechnology. *AIChE Journal*. 49(12): 2990-3006, 2003.

[40] Geyer FL, Ueda E, Liebel U, Grau N, Levkin PA. Superhydrophobic-Superhydrophilic Micropatterning: Towards Genome-on-a-Chip Cell Microarrays. *Angewandte Chemie International Edition*. 50: 8424-8427, 2011.

[41] Engberg K, Frank CW. Protein diffusion in photopolymerized poly(ethylene glycol) hydrogel networks. *Biomedical Materials*. 6:055006, 2011.

[42] Ingle JDJ and Crouch SR. *Spectrochemical Analysis*. Prentice Hall, New Jersey, 1988.

[43] Garoff H, and Ansorge W. Improvements of DNA sequencing gels. *Analytical Biochemistry*. 115:450-457, 1981.

[44] Dyanov HM, and Dzitoeva, SG. Method for attachment of microscopic preparations on glass for in situ hybridization, PRINS and in situ PCR studies. *BioTechniques*, 18:822-826, 1995.

[45] Grimson MJ, and Barker GC. A continuum model for the growth of bacterial colonies on a surface. *Journal of Physics A: Mathematical and General*. 26:5645-5654, 1993.

[46] Kreft JU, Booth G, and Wimpenny JWT. BacSim, a simulator for individual-based modelling of bacterial colony growth. *Microbiology*. 144(3275-3287), 1998.

[47] Gorochowski TE, Matyjaszkiewicz A, Todd T, Oak N, Kowalska K, Reid S, Tsaneva-Atanasova KT, Savery NJ. BSim: An Agent-Based Tool for Modeling Bacterial Populations in Systems and Synthetic Biology. *PLoS ONE.* 7(8): e42790, 2012.

[48] Kreft JU, Picioreanu C,Wimpenny JW, van Loosdrecht MC. Individual- based modeling of biofilms. *Microbiology.* 147:2897–2912, 2001.

[49] Centler F, Fetzer I, and Thullner M. Modeling population patterns of chemotactic bacteria in homogeneous porous media. *Journal of Theoretical Biology.* 287: 82-91, 2011.

[50] Keymer JE, Galajda P, Muldoon C, Park S, Austin RH. Bacterial metapopulations in nanofabricated landscapes. *Proceedings of the National Academy of Sciences of the United States of America.* 103(46): 17290-17295, 2006.

[51] Berg HC. *Random Walks in Biology*. Princeton University Press, Princeton, NJ, 1983.

[52] Berg HC. Turner L. Chemotaxis of bacteria in glass capillary arrays. *Biophysical Journal.* 58:919–930, 1990.

[53] Baba T, Ara T, Hasegawa M, Takai Y, Okumura Y, Baba M, Datsenko KA, Tomita M, Wanner BL, and Mori H. Construction of Escherichia coli K-12 in-frame, single-gene knockout mutants the Keio collection. *Molecular System Biology.* 2:0008, 2006.

[54] Wintermute EH, Silver PA. Emergent cooperation in microbial metabolism. *Molecular System Biology.* 6:407, 2010.

[55] Weiss R, and Knight T. Engineered Communications for Microbial Robotics. *Proceedings of the Sixth International Meeting on DNA Based Computers (DNA6).* June 2000.